SLAC-PUB-17633
February 18, 2022

Portal Matter and Dark Sector Phenomenology at Colliders

Thomas G. Rizzo †

SLAC National Accelerator Laboratory 2575 Sand Hill Rd., Menlo Park, CA, 94025 USA

arXiv:2202.02222v2 [hep-ph] 17 Feb 2022

Abstract

If dark matter (DM) interacts with the Standard Model (SM) via the kinetic mixing (KM) portal, it necessitates the existence of massive, likely $\gtrsim 1$ TeV, enabler portal matter (PM) particles that carry both dark and SM quantum numbers which will appear in vacuum polarization-like loop graphs. Such heavy states are only directly accessible at high energy colliders and apparently lie at mass scales beyond the direct kinematic reach of the ILC, CEPC and FCC-ee. A likely possibility is that these new particles are part of the 'next step' toward a UV-complete scenario describing both the SM and dark sector physics. A simple and straightforward example of such a scenario involving a non-abelian dark sector gauge group is employed in this work to demonstrate some of the range expected from this new physics. Here we present a broad survey of existing analyses designed to explore the nature of such PM states in a array of collider contexts, particularly at the LHC, and point out some of the future directions where additional work is obviously required in the hunt for new signatures as well as in model building directions.

†rizzo@slac.stanford.edu

1 Introduction and Background

Portals [1], sometimes represented as effective operators of various dimensions, are an efficient way to categorize broad classes of possible interactions between the visible states of the Standard Model (SM) and dark matter (DM) or, more generally, the various hidden states of the dark sector. Most of these portals can only function, however, if other new 'mixed' enabler states also exist. In the case of the well-studied, renormalizable, dimension-4 vector boson/kinetic mixing (KM) portal [1, 2], new enabling particles must exist which carry both SM and dark charges to generate the required loop-order, 2-point vacuum polarization-like graphs which are responsible for the KM. In the simplest case, where the low energy gauge interactions of the dark sector are described by an abelian $U(1)_D$ gauge group (under which all the SM particles are neutral, *i.e.*, have $Q_D = 0$) which kinetically mixes with the SM hypercharge, $U(1)_Y$, these new states, hereafter referred to as portal matter (PM) [3–7], must carry both hypercharge and also have $Q_D \neq 0$. Obviously, the KM setup itself critically relies upon the existence of such new particles, so one would do well to examine the nature of these hybrid PM states and learn what they can tell us more generally about DM and the physics of the dark sector. Since these particles carry SM quantum numbers, the only reason for them not to have already been observed is that they must be relatively massive, *i.e.*, likely $\gtrsim 1$ TeV for fermionic PM (with the details depending upon its color charge) and/or have atypical decays, as in the case of scalar PM, which makes present and future colliders the natural places to search for, discover and explore their properties. As noted, PM fields may be either fermionic, bosonic or more generally be some combination of both species and will more than likely also carry other additional SM quantum numbers besides the required hypercharge, *i.e.*, QCD color and/or $SU(2)_L$ weak isospin.

Of course, once we accept that PM states must exist, not only will they lead to obvious new physics when they can appear directly or indirectly in tree-level reactions, they can also lead to new loop-induced processes beyond the simple KM they were 'designed' to accomplish; such possibilities [8], including those in the flavor sector, have been to some extent previously discussed [4,6,7] and in many way are, *e.g.*, similar to the familiar vector-like fermion and multi-Higgs extensions of the SM. However, the fact that these fields now carry additional dark charges can make important alterations in the resulting phenomenology; the non-collider aspects of this physics are beyond the scope of the present work.

The study of PM can either be addressed from a bottom-up or from a top-down perspective - both from which we can glean important information about their apparent nature. In either case, however, at or below the weak scale where the effects of PM are indirect, the relevant physics is relatively straightforward and quite familiar. The PM fields at 1-loop order will generate a term in the Lagrangian of the form

$$\mathcal{L}_{KM} = \frac{\epsilon}{2c_w}\hat{V}_{\mu\nu}\hat{B}^{\mu\nu}\,, \tag{1}$$

where $\hat{B}^{\mu\nu}$ is the SM hypercharge gauge boson field strength tensor, $\hat{V}_{\mu\nu}$ is that for the analogous $U(1)_D$ gauge field tensor, *i.e.*, that of the dark photon (DP), $c_w = \cos\theta_w$, and ϵ if the strength of the KM generated by PM loops and is given by

$$\epsilon = c_w \frac{g_D g_Y}{24\pi^2}\sum_i\ \eta_i \frac{Y_i}{2} N_{c_i}\ Q_{D_i}\ ln\frac{m_i^2}{\mu^2}\,, \tag{2}$$

with $g_{Y,D}$ being the $U(1)_{Y,D}$ gauge couplings and $m_i(Y_i, Q_{D_i}, N_{c_i})$ are the mass (hypercharge, dark charge, number of colors) of the i^{th} PM field. Here, $\eta_i = 1(1/2)$ if the PM is a chiral fermion(complex scalar) and the hypercharge is normalized so that the electric charge is given by $Q_{em} = T_{3L} + Y/2$ as usual. In UV-complete theories, and as will be the case in the setups which we will be discussing below, the sum

$$\sum_i\ \eta_i \frac{Y_i}{2} N_{c_i} Q_{D_i} = 0\,, \tag{3}$$

so that ϵ is both finite and, if the PM masses are known, calculable within these frameworks and, for $O(1)$ mass splittings between the PM states, typically lying in the experimentally interesting range $\epsilon = 10^{-4} - 10^{-3}$. One trivially obvious statement that one can make from this is that the set of PM

fields *must* consist of more than a single state for such a cancellation as above to occur. We note that in what follows we will assume that the dark photon, V, acquires its mass via the vacuum expectation value(s) of one or more dark Higgs fields and that the masses of the DM, DP and the physical dark Higgs fields will all roughly lie in the interesting range below ~ 1 GeV. After applying field redefinitions to remove the KM, *i.e.*, $\hat{V} \to V$ and $\hat{B} \to B + \frac{\epsilon}{c_w} V$, to leading order in ϵ, and after spontaneous symmetry breaking of both the SM and the dark gauge group, the resulting $Z - V$ mass mixing matrix can be easily diagonalized. One then finds that for masses in the range, $m_V^2/m_Z^2 << 1$, the DP will couple to the SM fields in the expected fashion, as $\simeq e\epsilon Q_{em}$, to leading order in the small parameters, with e being the proton's charge. It is important to note that ϵ depends only upon the *ratios* of the masses of the PM states and not on their specific masses so that ϵ itself provides no obvious guidance as to where to look for the actual PM particles. However, as we will see below, in the case of a simple scalar PM scenario at least, one finds that there can be additional model-dependent restrictions on the spectrum of PM masses due to the requirements of electroweak symmetry breaking in the SM.

However, one reason that we might expect that the PM states, as well as a more complex dark gauge sector, may not be too far away in energy above the weak scale (at least for part of the parameter space where the DM coupling is somewhat large) is to consider the running of the dark gauge coupling, g_D or more precisely below, $\alpha_D = g_D^2/4\pi$. As is well-known, a $U(1)$ gauge theory is not asymptotically free and eventually will become strongly coupled or even have a Landau pole at some point as the energy scale increases. Here, we will take advantage of this observation noting that in a UV-complete theory one would expect new physics of some form to enter before either of these things can happen. In order to be specific for demonstration purposes, let us consider the case of light fermionic DM, having $Q_D = 1$, together with the DP and dark Higgs all lying in roughly the same mass range ~ 100 MeV. To be even more specific, and in order to avoid direct detection bounds due to inelastic DM scattering as well as the strong constraints from the CMB [9–12] for fermionic DM in this mass range, we consider the scenario where the DM is pseudo-Dirac with the relevant mass splitting generated by the same dark Higgs vev that is responsible for the mass of the DP. Assuming that these few fields are the only light states, we can then run the value α_D in a known manner from this low energy scale, M_L, up to some higher scale, M_U (or until some new physics with $Q_D \neq 0$ enters the RGE's) where one reaches a region of strong coupling or even hits a Landau pole[1]. Recall that the SM fields will *not* enter into this calculation as they all have $Q_D = 0$ and so will not couple to the DP to LO in the $\epsilon \to 0$ limit. The results of these simple considerations can be found in Fig. 1 from [13]. In this Figure, we can see that if $\alpha_D(M_L) \geq 0.175(0.20)$, a not infrequent assumption made in many phenomenological analyses [14–17], its value will become non-perturbative (or even hit a Landau pole [18]) before $M_U \simeq$ a few TeV when running up from the $M_L = 100$ MeV scale. Semi-quantitatively, we see that these results are not very dependent as to whether they are obtained at the 1-, 2- or 3-loop level as can be gleaned from this Figure. Although these results are only indicative, they give some credence to the likelihood that the PM fields and an associated more complex, non-abelian dark sector gauge structure, *e.g.*, an $SU(2)_D$ [4, 7, 19], are likely not to be too far above the weak scale and may be accessible at the HL-LHC and at other planned future colliders.

In this White Paper, we will examine some of the generic phenomenological implications of a set of 'relatively simple' PM models and their associated dark sectors which will act as guideposts to the physics scenarios resulting from the more realist and complex scenarios that may appear in a fully UV-complete KM model. The possibilities here are rather wide ranging and so it should be noted that much of this work is still in progress so that only preliminary results are available in some cases at this point. We will, however, rely *quite* heavily on the results as presented in earlier analyses [3, 4, 6, 7] for much that appears below.

The outline of this paper is as follows: In Section 2, we review some basic ideas and mechanics behind the setup for a simple low-scale $U(1)_D$ fermionic PM scenario; here the PM fields must be heavy, vector-like copies of the usual SM fermion representations to allow for the PM to decay reasonably quickly to agree with cosmological constraints. In Section 3, we consider one example of a more UV-complete scenario of PM with an enlarged dark sector gauge group, based on an E_6-inspired framework, which embodies the previously discussed simple model but with a highly enriched phenomenology. Section 4

[1] Any additional light fields with $Q_D \neq 0$ will only strengthen these arguments below since then α_D will only run more quickly.

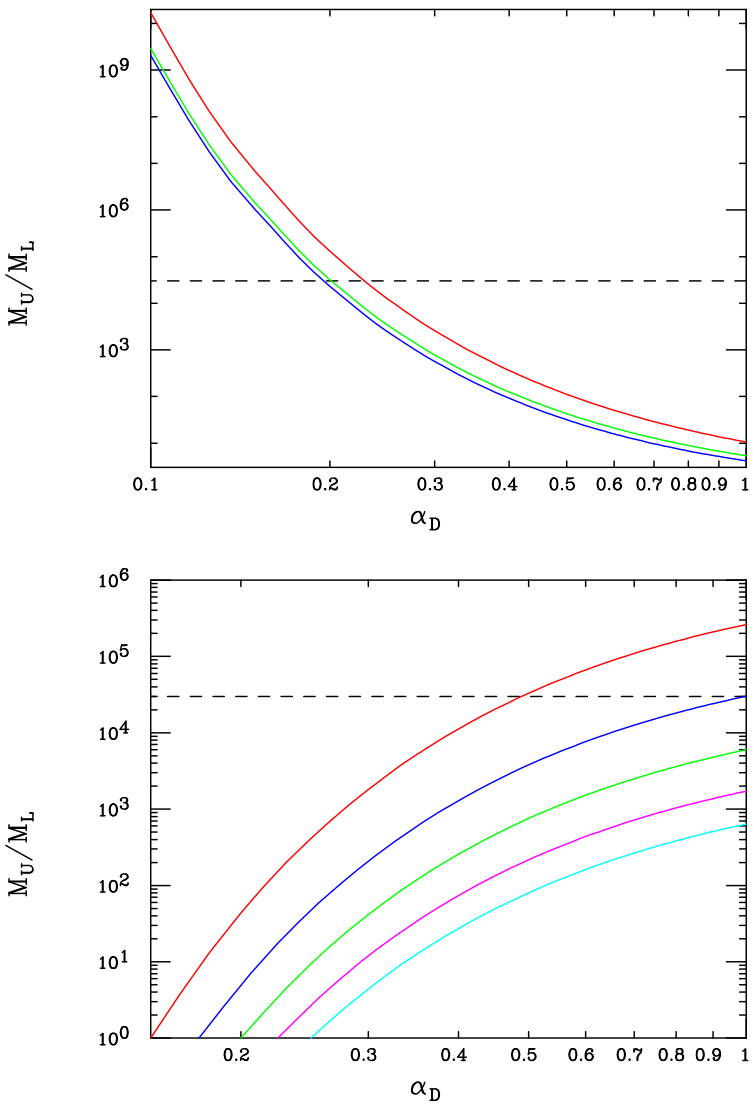

Figure 1: The running of α_D in the pseudo-Dirac DM example discussed in the text. The top panel shows the location of the Landau pole, M_U, at the 1-loop(red), 2-loop(blue) and 3-loop(green) level in RGE running, employing the $\bar{M}S$ scheme, as a function of $\alpha_D(M_L)$ where M_L is the low scale associated with the DM, DP and dark Higgs fields, $\simeq 100$ MeV. The dashed line corresponds to $M_U = 3$ TeV when $M_L = 100$ MeV as a guide for the eye. The lower panel shows the 3-loop running of α_D (on the x-axis) in this same scenario as a function of M_U/M_L. The curves, from top to bottom, are for $\alpha_D(M_L) = 0.15, 0.175, 0.20, 0.225$ and 0.25, respectively. Here we see that, *e.g.*, if $\alpha_D(M_L = 100 \text{ MeV}) \geq 0.175$ then $\alpha_D \geq 1$ for $M_U \geq 3$ TeV, again indicated by the dashed line.

contains a broad overview and discussion of some of the $e^+e^-, \gamma\gamma$ and LHC signatures for this scenario, reviewing several past studies and pointing out where more work is clearly needed. Section 5 contains a discussion of the phenomenology of an alternative scalar PM model where additional scalar doublets carrying dark charges act as as both the dark Higgs fields breaking $U(1)_D$ as well as PM. Finally, in the last Section we summarize the essential results and conclusions as well as point out some possible future directions.

2 Simple Ideas and Basics

For simplicity we begin our discussion assuming PM is fermionic and that the relevant gauge group below the mass scale of the PM fields themselves, $\lesssim 1$ TeV, is simply $G_{SM} \times U(1)_D$. In such a case, the PM fermions must be vector-like, *i.e.*, VLF's, with respect to both gauge groups in order to avoid anomalies, constraints from electroweak fits [20] and unitarity [21], as well as having any significant contribution to the Higgs to $gg/\gamma\gamma$ partial decay widths which would be the case of, *e.g.*, a fourth generation of *chiral* fermions. At the electroweak scale or below, being vector-like, these PM fermions are allowed to have (apparent) bare mass terms and thus are not generated by their couplings to the SM Higgs. Of course in a more UV-complete theory such masses might be generated by, *e.g.*, the Higgs fields that are responsible for the breaking of a larger dark gauge group, G_{dark} down to $U(1)_D$. Since the PM fields carry $Q_D \neq 0$ as well as hypercharge, the lightest among them will be stable unless they are allowed to mix with one or more of the lighter SM fermion fields, *i.e.*, $f = (\nu, e)^T_L, (u, d)^T_L, e_R, u_R, d_R$ (suppressing the generation index) through, *e.g.*, the vev of a complex isosinglet dark Higgs field, h_D, which may or may not also be the dominant source of the DP's mass. This implies that the PM fields, F, must transform in a vector-like manner [22] similar to one or more of these SM fermion representations, *i.e.*, $F = (N, E')^T, (U', D')^T, E, U, D$ (again dropping any potential generation indices) with the primes only being employed here to help distinguish isosinglet from isodoublet fermions with the same electromagnetic and color charges. Of course, one can also imagine dark Higgs fields which can transform as $SU(2)_L$ doublets as long as their vevs are sufficiently suppressed to below the $\lesssim 1$ GeV level to avoid other constraints. In a general scenario, one may easily imagine that dark Higgs fields of both varieties may be present simultaneously as will be realized in a particular manifestation below.

Perhaps, the very simplest toy model/bottom-up example [3] that we can construct from the observations above, which we will analyze as a test case for demonstration purposes, is then that the set of PM fields consisting of just two $Q_D = \pm 1$, weak isosinglets states having $Q_{em} = -1$, *i.e.*, $E_{1,2}$ (assumed to be colorless), with comparable but somewhat different masses, $m_1 \lesssim m_2$, thus rendering ϵ finite and calculable; specifically, for this color singlet scenario one obtains

$$|\epsilon| \simeq 3.0 \left(\frac{g_D}{0.3}\right) \frac{ln(m_2/m_1)}{ln\ 1.5} \cdot 10^{-4} \tag{4}$$

as desired. The E_i may be thought of as vector-like copies of the RH-electron (or muon or tau, but we will use the electron in this simple toy example) and if we take $|Q_D(h_D)| = 1$ as well, then an off-diagonal $f - F$-type interaction can be generated of the form

$$\mathcal{L}_{Mix} = \ \lambda_1 \bar{E}_{1L} e_R h_D + \lambda_2 \bar{E}_{2L} e_R h_D^\dagger + h.c. \tag{5}$$

where the λ_i are presumably $O(1)$ Yukawa couplings and, again, all potential generation indices have been suppressed. A very similar expression can obviously be written in the case of, *e.g.*, weak isosinglet quarks. Now, when the complex field, h_D, acquires a vev, *i.e.*, $h_D \to (v_s + S + iA)/\sqrt{2}$, $v_s \neq 0$, it generates mass mixing between the PM fields and, in this example, the SM electron. It is important to note that the mixing that is induced is with, *e.g.*, the RH-electron so that these interactions are *chiral*. If the PM fields had *instead* been chosen to be two sets of the color-singlet, weak isodoublets, $(N, E')^T_i$, then the corresponding chiral coupling would then be with the LH-electron through the same h_D isosinglet dark Higgs, *i.e.*, the mixing is generated between states with the *same* weak isospin as h_D is here assumed to be isosinglet, *i.e.*, h_{D_S}. This simple result can be seen to be easily generalizable to cover all of the other potential scenarios for various specific choices of the PM fields; of course, in a more UV-complete

picture something more complex is possible as we will see below. For example, if the dark Higgs involved in the coupling had instead been an isodoublet then the helicity of these couplings would then have been reversed. Note that when h_D is the same (and, in the toy example here, only) scalar which generates the DP mass, the CP-odd field, A, then becomes the Goldstone boson, G_V, associated with the DP's longitudinal degree of freedom and the CP-even state, S, is the remaining *physical* dark Higgs. Of course, more generally, if multiple dark Higgs fields are present, A, will become an admixture of this Goldstone and a (set of) physical CP-odd mass eigenstate(s), *etc*, as one sees, *e.g.*, in the Two-Higgs Doublet Model. Similarly, the light dark Higgs mass eigenstate will also become some admixture of the various CP-even fields in this more complex scalar sector.

Following this through, it should then be noted that in more general, and likely more realistic, models the dark Higgs fields with $Q_D \neq 0$ that transform non-trivially under $SU(2)_L$, *e.g.*, as isodoublets, may also appear in the spectrum as noted above. Their vevs will also contribute to the mass of the DP so are likewise constrained to be rather small in the present setup, $\lesssim 1$ GeV, but this remains sufficient to now influence $V - Z$ mass mixing as well as the general mixing between the PM and SM fields. Clearly, the choice of the $SU(2)_L$ representation(s) of the PM fields will also directly influence the dark Higgs' $SU(2)_L$ transformation properties if we want to maintain gauge invariant couplings that allow all the PM fields to decay. One can symbolically summarize all of these possible couplings for the color singlet, $Q_{em} = -1$, PM fields via the generalized PM-SM mixing Langrangian

$$\mathcal{L}'_{Mix} = \lambda_S \bar{E}_L e_R h_{D_S} + \lambda'_S (\bar{\nu}, \bar{e})^T_L (N, E')^T_R h^\dagger_{D_S} + \lambda_D (\bar{\nu}, \bar{e})^T_L E_R h^\dagger_{D_D} + \lambda'_D (\bar{N}, \bar{E}')^T_L e_R h_{D_D} + h.c. \quad (6)$$

where, using the notation above, $h_{D_{(D,S)}}$ here represents the weak $SU(2)_L$ isodoublet or isosinglet dark Higgs field, respectively, and the λ's are again assumed to be $O(1)$. Note the primed and unprimed fields in this expression. As in the previous example, analogous interaction terms can straightforwardly be written down for other PM quantum number choices.

In the form written above we have suppressed any flavor issues and one may ask if the PM couples predominantly only to a single generation (in some limit), mixes with all three SM generations, or whether or not the PM themselves come in three generations. Clearly, some more than others of these scenarios will be strongly constrained by experimental results for the flavor sector. All of these possibilities appear in the literature [4] but it is beyond the scope of the present work to provide an overview of all of them especially as we are here more focussed on the collider aspects of PM models. However, flavor issues will enter the discussion when they are clearly relevant to specific experimental signatures and production mechanisms so here we'll usually assume that the simplest possibilities are realized.

Let us now return to the simple isosinglet dark Higgs model above with isosinglet, colorless PM fermions. As is easily seen, interactions such as $\mathcal{L}_{Mix}$ will allow for the generic PM decays of the form $F \to f(S, V = V_{long} \simeq G_V)$, with rates controlled by the $O(1)$ values of the λ_i parameters. The Goldstone Boson Approximation [23] limit is applicable here as $m^2_{S,V} << m^2_F$ since all the PM fermion masses must clearly be at least several hundreds of GeV or more in order to have so far evaded experimental detection. It is easy to see in this same Goldstone limit that $\Gamma(F \to fS) = \Gamma(F \to fV)$ provided that $m^2_f << m^2_F$ which will always be the case except, perhaps, when $f = t$. One explicitly finds in this limit that

$$\Gamma(F_i \to fV, fS) \simeq \frac{\lambda_i^2 m_i}{64\pi}\,, \quad (7)$$

under these assumptions. As is well-known, the SM-like Higgs-induced mixing of heavy vector-like fermions with analogous SM fields with the *opposite* value of the weak isospin (*e.g.*, singlets with doublets), such as $E'_L - e_L$ and not $E_L - e_L$ type mixing, would also yield the more familiar decays $F \to f'W, fZ$ and fh_{SM} which are usually anticipated in performing vector-like fermion searches at the LHC. Here, such couplings will be immediately induced once the $F - f$ mass matrix is diagonalized [3,5]. In the case of an isosinglet F, in the approximation that $m^2_{f,f',W,Z,h_{SM}} << m^2_F$ then the partial widths to these final states are related with the usual result being $\Gamma(W) = 2\Gamma(Z) = 2\Gamma(h_{SM})$, for F being an isosinglet (the W mode is absent in the isodoublet case) and are highly suppressed by the square of the relevant $F_i - f$

mixing angle, here $\sim \theta_{L_i}^2 << 1$, so that, *e.g.*,

$$\Gamma(F_i \to f h_{SM}) \simeq \frac{G_F m_i^3}{16\sqrt{2}\pi}\theta_{L_i}^2 \,, \tag{8}$$

with G_F being the Fermi constant, while the corresponding partial widths to $S, V \simeq G_V$ final states experience no such suppression and are instead proportional to the λ_i^2, which are expected to be of $O(1)$, as noted above. However, the λ_i themselves at some level control the size of the $F - f$ mixing. Thus, we should expect that the decays of the PM fields, F's, into dark sector fields will always be (very) far dominant which makes their production signature different from ordinary VLF's. This implies that it will be the decays of S and V, which essentially always appear as final states in F_i decay, that will determine the collider signature for PM production.

Once a PM $\bar{F}F$ pair is produced from an e^+e^-, $\bar{q}q$ or gg initial state collision and then decays, the resulting final state will be a simple admixture of $\bar{f}f + 2V, 2S, SV$ with the $\bar{f}f$ appearing as either a opposite-sign, same flavor lepton pair or a pair of jets (or possibly missing energy if $f = \nu$). The more complex issue is what will V, S decay into: as is well-known, this is essentially determined by the relative masses of V, S and the DM fields. If $m_V > 2m_{DM}$, since the DM is stable, V will decay invisibly to DM pairs with a rate proportional to $\sim g_D^2$; if this condition is not satisfied then V will instead visibly decay into pairs of SM fields, *e.g.*, e^+e^-, $\mu^+\mu^-$, *etc*, although such decays are suppressed in rate by $\sim \epsilon^2$. If $m_S > 2m_V$ then $S \to 2V$ happens quickly and will dominate whereas if $2m_V > m_S > m_V$ then S decays as $S \to VV^*$ and can be potentially relatively long lived. This will certainly be the case if $m_S < m_V$ so that the completely off-shell, $S \to V^*V^*$, and the loop- or mixing-induced, *e.g.*, $S \to e^+e^-$ [24], decays are relevant. Thus we must conclude that S, V will either materialize as missing energy or highly boosted lepton-jets [3, 25]. For example, in the case of the missing energy mode, the existing LHC searches for Supersymmetry involving jets and/or leptons + MET can be recast for the case of $\bar{F}F$ production if S, V decay invisibly which then tells us that in such a scenario, *e.g.*, $m_{E(E')} \gtrsim 0.90(1.05)$ TeV [26–28] for first/second generation-like isosinglet E (isodoublet E') and $m_Q \gtrsim 1.3 - 1.5$ TeV [3,5], depending on the final state fermion flavor, values which are beyond those directly accessible to the ILC, CEPC or FCC-ee, as we will discuss further below. For third generation-like color-singlet PM the prospects for obtaining comparable constraints are somewhat poorer [29, 30]. It is to be noted, however, that if the PM fields exist within a more complex scenario, such as those we will touch upon below, where, *e.g.*, the dark gauge group may be enlarged, then at least the more massive PM fields may be allowed to suffer other decay paths than those discussed above. A simple version of such setup will be discussed in the next Section but we will see that in a significant part of the parameter space the essential phenomenology returns to this simple picture that we have so far described.

Although this basic scenario is perhaps adequate as an effective theory at the weak scale and below, it does not on its own provide much guidance as to how or if the PM and SM fields may fit together is some type of more common framework. We will return to this issue from a specific perspective below, mostly concentrating on one possible next step up the ladder in the bottom-up approach.

3 An Example of a More UV-Complete PM Scenario

Outside of the direct production of the PM fields themselves at colliders via SM processes, *i.e.*, the usual QCD and electroweak interactions, the simple toy examples above do not lead to any 'unusual' phenomenology other than MET and/or displaced vertices. However, if we take another step upward in the ladder to a UV-complete theory this is no longer true. Perhaps one of the most interesting paths is to imagine enlarging the dark gauge group beyond $U(1)_D$, *i.e.*, to a more general G_{dark} which is a single non-abelian group or is a product group with non-abelian and/or abelian factors. A full UV-complete picture would then have a 'unified' group, G_U break down to, *e.g.*, $G_{SM} \times G_{dark}$ at some large scale followed by G_{dark} breaking to $U(1)_D$ at, say, ~ 10 TeV. Of course, one can imagine all sorts of ways to grow the dark gauge group itself, *e.g.*, a dark gauge group 'orthogonal' to SM [13], as an extension of the SM electroweak sector [4], as a unification with an enlarged gauged flavor symmetry group [7], or even combined with QCD into a single larger group [19]. Clearly, any new physics signatures will depend to

some extent upon which of these paths, if any, might be chosen by nature.

Table 1: Fermionic Field Content

SU(5)		$SU(3)_C$	T_{3L}	$Y/2$	T_{3I}	$Y_I/2$	Q_D
10	$Q \equiv \begin{pmatrix} u \\ d \end{pmatrix}_L$	**3**	$\begin{pmatrix} 1/2 \\ -1/2 \end{pmatrix}$	1/6	0	0	0
	u_L^c	$\bar{\mathbf{3}}$	0	-2/3	0	0	0
	e_L^c	**1**	0	1	0	0	0
$\bar{\mathbf{5}}$	$L \equiv \begin{pmatrix} \nu \\ e \end{pmatrix}_L$	**1**	$\begin{pmatrix} 1/2 \\ -1/2 \end{pmatrix}$	-1/2	1/2	-1/2	0
	d_L^c	$\bar{\mathbf{3}}$	0	1/3	1/2	-1/2	0
$\bar{\mathbf{5}}$	$H \equiv \begin{pmatrix} N \\ E \end{pmatrix}_L$	**1**	$\begin{pmatrix} 1/2 \\ -1/2 \end{pmatrix}$	-1/2	-1/2	-1/2	-1
	D_L^c	$\bar{\mathbf{3}}$	0	1/3	-1/2	-1/2	-1
5	$H^c \equiv \begin{pmatrix} E \\ N \end{pmatrix}_L^c$	**1**	$\begin{pmatrix} 1/2 \\ -1/2 \end{pmatrix}$	1/2	0	1	1
	D_L	**3**	0	-1/3	0	1	1

3.1 A UV-Inspired Model Framework

Ref. [4] provides a basic E_6-inspired setup in this direction with some interesting collider phenomenology. At the level relevant for our discussion here, in this example the dark gauge group is effectively enlarged to $SU(2)_I \times U(1)_{I'} \equiv 2_I 1_{I'}$, which is qualitatively similar in nature to the SM, and is broken down to $U(1)_D$ at a multi-TeV scale. As we will see (but not make use of here) this $2_I 1_{I'}$ group structure and $U(1)_D$ quantum number assignments are such that this dark product group might be embeddable into $SU(3)_I$ at an even higher mass scale. Here the gauge couplings are simply $g_I, g_{I'}$, respectably, and we identify the $U(1)_D$ gauge coupling above as $g_D = e_I = g_I \sin\theta_I$ with $x_I = \sin^2\theta_I$ being the analog of the usual SM weak mixing angle, $x_w = \sin^2\theta_w$, of *a priori* unknown value which depends upon the full UV-completion of the model. In such a setup, $Q_D = Q_I = T_{3I} + Y_I/2$, as one might expect. Due to the E_6-inspired nature of this scenario, the 'exotic' PM fields form (at least) a complete $\mathbf{5} + \bar{\mathbf{5}}$ of the familiar $SU(5)$ with $Q_D = 1, -1$, respectively, so that $Q_D(D) = 1$ while $Q_D(N, E) = -1$; other fermions which are SM singlets, *e.g.*, the ν_R, S_L fields which fill out the usual **27** of E_6 [31] as well as other exotics, will also be present and may be necessary to, *e.g.*, cancel gauge anomalies and also insure that ϵ is finite[2]. This basic matter content for this scenario is schematically shown in Table 1; note that in this setup $(d_L, D_L)^c$ and (L_L, H_L) are doublets under $SU(2)_I$ with the latter actually being a bidoublet under $SU(2)_L \times SU(2)_I$, similar to what is encountered in the Left-Right Symmetric Model. Thus, $SU(2)_I$ is seen to directly link the D_L^c and H_L, $Q_D \neq 0$ PM fields with the corresponding d_L^c and L_L fields of the SM both having $Q_D = 0$. In such a setup, the role of Q_D in the KM expressions above is now replaced by the combination $Q_D \to c_I Y_I/2$ since it is $1_Y 1_{I'}$ whose corresponding gauge fields now undergo dim-4 KM, appearing symmetrically with (so far the fermionic contribution) $TrYY_I = 0$ thus insuring that ϵ is finite.

Since this scenario is E_6-inspired and, as seen from Table 1, a single generation of the SM and PM fields fit into a **27** representation of this group, one may ask whether or not there is only a single set of the PM fields or there is one set for each SM generation, as would perhaps be the naive E_6 expectation. As noted above, there are clear flavor physics aspects to this choice which we will only explore from the collider side here. Note that while vector-like with respect to the SM, under $2_I 1_{I'}$, the PM fields are *not* vector-like so that dark Higgs fields are necessary to generate their masses. In fact, we needs multiple Higgs fields with the appropriate transformations properties but which have vevs at the ~ 10 TeV, ~ 100

[2]For clarity we will here use first generation labels for all the fields as we have in the previous Section.

Table 2: Higgs Sector Content

Φ	$SU(2)_L$	$Y/2$	$SU(2)_I$	$Y_I/2$	$\langle\Phi\rangle$
H_1	**2**	1/2	**1**	0	$\frac{1}{\sqrt{2}}\begin{pmatrix}0\\ v\end{pmatrix} \sim \begin{pmatrix}0\\ 100\text{ GeV}\end{pmatrix}$
H_2	**2**	-1/2	**2**	1/2	$\frac{1}{\sqrt{2}}\begin{pmatrix}v_1 & v_2\\ 0 & 0\end{pmatrix} \sim \begin{pmatrix}1\text{ GeV} & 100\text{ GeV}\\ 0 & 0\end{pmatrix}$
H_3	**1**	0	**2**	-1/2	$\frac{1}{\sqrt{2}}\begin{pmatrix}v_3 & v_4\end{pmatrix} \sim \begin{pmatrix}10\text{ TeV} & 1\text{ GeV}\end{pmatrix}$

GeV and ~ 1 GeV scales. The minimal content of the (fine tuned) Higgs sector that accomplishes the required symmetry breaking at these mass scale is then given in Table 2 and is discussed in detail in Ref. [4]. Additional scalars without vevs may need to be present to maintain a finite ϵ and/or to act as a low mass scalar DM candidate. Once these three Higgs fields obtain the various vevs as shown in the Table, numerous new collider signatures are found to be generated.

The vev v_3 is the one responsible for the $2_I 1_{I'} \to 1_D$ breaking, generating the dominant contribution to the masses of the Z_I and $W_I^{(\dagger)}$ gauge bosons as well as the dominant mass terms for the N, E and D PM fermion fields. Here we note that while Z_I has $Q_D = 0$, but one finds instead that the $Q_{em} = 0$, but non-hermitian, fields $W_I^{(\dagger)}$, carry $Q_D = \pm 1$. In such a setup the analog of the SM photon after the breaking the $2_I 1_{I'} \to 1_D$, which we might call A_I, can be easily identified with the DP, *i.e.*, V, discussed above. In the $v_3^2 >> v^2, v_{1,2,4}^2$ and $\epsilon \to 0$ limits, as expected one finds the SM-like results that $m_{W_I} = g_I v_3$ and $m_{Z_I} = m_{W_I}/c_I$, *i.e.*, the analogous $\rho_I = 1$ at tree-level due to isodoublet breaking but may suffer from significant loop effects here due to large mass splittings within the $SU(2)_I$ fermion representations, in principle. The gauge fields in this same limit couple in a manner completely analogous to the corresponding ones in the SM with the obvious substitutions, *e.g.*, $L \to I$. Similarly, in the $v^2, v_2^2 >> v_{1,4}^2$ and $\epsilon \to 0$ limits, the SM gauge fields obtain there masses similarly to what happens in the Two Higgs Doublet Model(2HDM), *i.e.*, $m_W^2 = g^2(v^2 + v_2^2)/4 = m_Z^2 c_w^2$. Of course, all these vevs are non-zero as is ϵ so that the gauge boson mass matrices are much more complex; we can, however, adequately work to lowest order in $\epsilon \sim 10^{-(3-4)}$ and in the ratios of the squares of the various vevs. This leads to several interesting effects[3]: (*i*) We observe that that the u mass (and a possible a ν Dirac mass) is generated by v while the d, e masses are generated by v_2 similar to the 2HDM. (*ii*) The SM Z and the Z_I are found to (mass) mix by a small angle, *i.e.*,

$$\theta_{ZZ_I} \simeq \frac{g_I/c_I}{g/c_w}\,\frac{m_Z^2}{m_{Z_I}^2}\,\frac{v_2^2}{v^2+v_2^2}\,, \tag{9}$$

where the last ratio of vevs is similar to the $\cos^2\beta$ factor in the 2HDM, and is expected to be $O(1)$. (*iii*) The SM Z mixes with the DP, $V = A_I$, in this language, by a small angle

$$\theta_{ZA_I} \simeq -\epsilon t_w + \frac{g g_I s_I}{2c_w}\,\frac{v_1^2}{m_Z^2} \equiv -\epsilon t_w + \sigma\,, \tag{10}$$

which is induced by both KM and mass mixing. Note that the ratio of these two contributions, $r_0 = \sigma/(\epsilon t_w)$, is also expected to be $O(1)$ for typical choices of parameter values:

$$r_0 \simeq 0.26\left(\frac{10^{-4}}{\epsilon}\right)\left(\frac{v_1}{1\text{GeV}}\right)^2\left(\frac{g_I s_I}{g s_w}\right). \tag{11}$$

(*iv*) The mass of the DP in the eigenstate basis to leading order in the small mixings is now given by

$$m_{V=A_I}^2 = g_I^2 s_I^2 v_1^2 + \sigma(2\epsilon t_w - \sigma) m_Z^2\,. \tag{12}$$

[3]For details, see Ref. [4].

where, quite generally, the first term is dominant for masses $\geq 50-100$ MeV; note the absence of v_4 here. (i) Recalling that $g_D = e_I = g_I s_I$ and $Q_D = Q_I$, the DP is now found to couple to the combination

$$g_D Q_D + e\epsilon Q_{em} - \sigma \frac{g}{c_w}(T_{3L} - x_w Q_{em})\,. \tag{13}$$

While the first two vector-like terms are as above in the previous Section, here we see that the DP has an additional coupling to the SM fields proportional to that of the SM Z boson, a well-known side effect of there being a dark Higgs field that obtains a vev while also carrying ordinary weak isospin, here being an $SU(2)_L$ isodoublet, *i.e.*, $v_1 \neq 0$.

As in the toy example, the set of Higgs fields in Table 2 not only generate masses for the SM and PM fermions but also the mixings in the, *e.g.*, $d-D$ and $e-E$ sectors as discussed in detail in Ref. [4]. These terms produce (almost) calculable values for the corresponding λ couplings for the light dark Higgs and the DP's Goldstone boson which appeared in the last Section up to $O(1)$ parameter ratios, *e.g.*,

$$\lambda_{E,D} = \sqrt{2}\left(\frac{v_4}{v_1}\right)\left(\frac{2m_{E,D}}{v_3}\right) = 0.42\left(\frac{v_4}{v_1}\right)\left(\frac{m_{D,E}}{1.5\text{TeV}}\right)\left(\frac{10\text{TeV}}{v_3}\right) \sim O(1)\,, \tag{14}$$

where v_4/v_1 is the ratio of the two $U(1)_D$ breaking vevs and here we see that these λ's are indeed naturally $O(1)$ in this setup.

4 Collider Signature Survey

4.1 e^+e^- Colliders

The initial run of the ILC [32] at $\sqrt{s} = 240$ GeV and/or the FCC-ee/CEPC at $\sqrt{s} = 240-380$ GeV [33,34] do not allow for the on-shell production of any of the new PM fields discussed in the previous section as their masses likely lie $\gtrsim 1$ TeV, so, at best, we must concentrate on their indirect effects which are not suppressed by powers of ϵ or by tiny mixing angles given the available integrated luminosities. Similar kinematic constraints would apply for low energy $\gamma\gamma$ colliders [35] although they may have access to different PM sensitivity channels. As noted, since the direct production of PM states cannot occur, we concentrate on the the production of the light V, S states. Traditionally at e^+e^- colliders [36, 37], one employs the $e^+e^- \to V\gamma$, ϵ^2-suppressed process to search for the DP, but here we can take advantage of the higher center of mass energies to examine the $e^+e^- \to 2V(2S)$ and $e^+e^- \to VS$ processes. These reactions can now occur through $t-, u-$channel E exchange suffering no ϵ-dependent coupling suppressions with rates proportional to λ_E^4 with $\lambda_E = \lambda$ being $O(1)$ as discussed above. The V that appears in this case is essentially the longitudinal component of $V_L \simeq G_V$ via the Goldstone Theorem. Here we will initially assume that both S and V materialize as boosted, but with otherwise visible, decay products in the e^+e^- collider detector.

The cross sections for the processes $e^+e^- \to 2V(2S)$ are identical in the $m_{S,V} \to 0$ limit that we consider, since $m_{V,S}^2 << s$, and are given by (in the Goldstone Boson Approximation)

$$\frac{d\sigma_{2V,2S}}{dz} = \frac{\lambda^4}{256\pi s}\,\frac{z^2(1-z^2)}{(a^2-z^2)^2}\,, \tag{15}$$

where $a = 1 + 2m_E^2/s$ and $z = \cos\theta^*$, the center of mass scattering angle, while the corresponding cross section for $e^+e^- \to VS$ is given by (in the same limit)

$$\frac{d\sigma_{VS}}{dz} = \frac{\lambda^4}{128\pi s}\,\frac{a^2(1-z^2)}{(a^2-z^2)^2}\,. \tag{16}$$

Note that since $4m_E^2 >> s$ for the PM mass range of interest to us and the ILC and FCC-ee/CEPC center of mass energies above, $a >> 1$ so that both cross sections will peak at large angles and that the integrated cross section $\sigma_{2V,2S} \sim (\sqrt{s}/2m_E)^8$ while that for the VS final state instead scales as

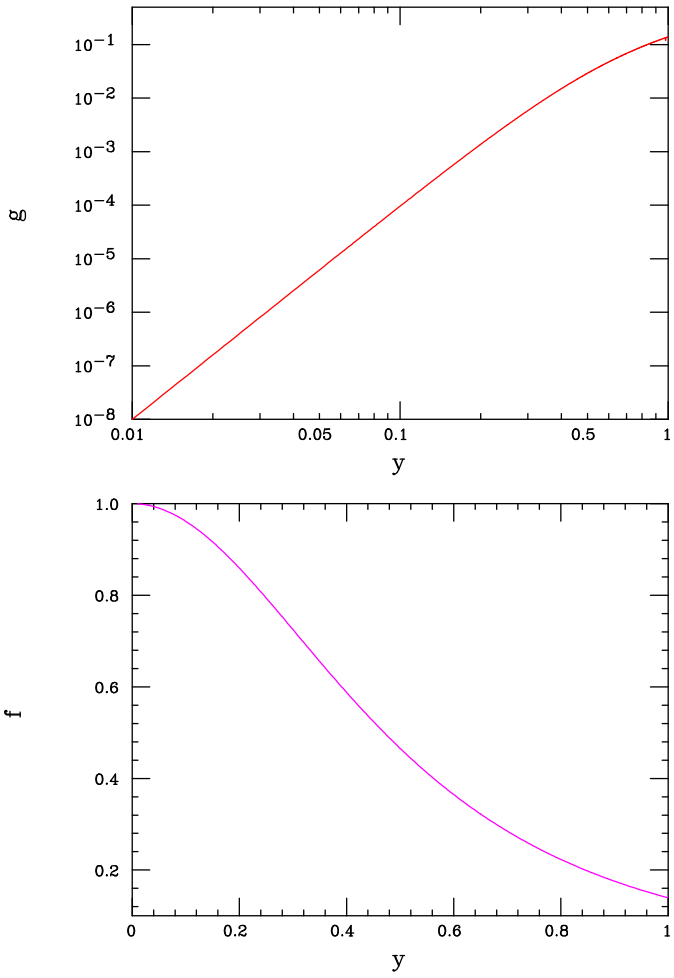

Figure 2: The kinematic functions $g(y)$ (top) and $f(y)$ (bottom), as defined in the text, as functions of $y = \sqrt{s}/(2m_E) < 1$.

$\sigma_{VS} \sim (\sqrt{s}/2m_E)^4$ and is thus significantly larger so that we will mainly be interested in this process. To emphasize this scaling behavior we can write this total cross section as

$$\sigma_{VS} = \frac{\lambda^4}{24\pi s}\Big(\frac{\sqrt{s}}{2m_E}\Big)^4 \; f(y)\,, \tag{17}$$

where $f(y) = y^{-4}g(y)$ with $y = \sqrt{s}/(2m_E)$ and, writing $a = 1 + (2y^2)^{-1}$ we find that

$$g(y) = \frac{3}{16}\left[\frac{1}{2}(a + a^{-1})\log\Big(\frac{a+1}{a-1}\Big) - 1\right]. \tag{18}$$

The functions f and g are shown in Fig. 2 where as expected we see that f is essentially $O(1)$ over the kinematic range of interest while g displays the very strong power-law dependence of the total cross section on y. The $e^+e^- \to SV$ cross section can be rather significant; indeed, assuming that $\sqrt{s} = 240(380)$ GeV, one obtains $\sigma_{VS} \simeq 7.9(5.8)[\lambda^4 g(y)] \cdot 10^4$ fb. This implies that even if the product $\lambda y \lesssim 0.1$, a substantial event sample will be obtainable when integrated luminosities on the order of $\mathcal{L} \sim$ a few ab^{-1}

are achieved. For completeness we note that under the same set of assumptions, $\sigma_{2S,2V}$ is smaller by a factor of $\sim y^4 \sim 10^{-4}$ and is indeed unobservably small.

So far we have assumed that S, V materialize as visible objects in the detector but if they are long-lived or V decays to DM then there is no way to really observe such events. The usual approach, which we follow here, is then to require an ISR photon as a tag as part of the SV production process which will clearly reduce the event rate before cuts by a factor of order $\sim (\alpha/\pi) log(s/m_e^2)$. The final state will now appear as arising from $e^+e^- \to \gamma$+missing energy which has a significant well-known background from the SM process $e^+e^- \to \gamma\bar{\nu}\nu$ arising from s-channel Z exchange as well as $t-$channel W exchange when $\nu = \nu_e$. The resulting cross section assuming that, *e.g.*, $\lambda_E = 1$ and for fixed values of $\sqrt{s}$ and m_E is then directly obtainable; the results of this calculation are shown in Fig. 3 for $d\sigma_{SV}/dx_g$, where $x_g = 2E_\gamma/\sqrt{s}$. Also shown here in the integrated cross section above a given minimum cut on the photon energy, *i.e.*, x_g^{min}, for the same values of the other parameters. Here one sees that the shape of the photon energy distribution is as expected from a typical ISR process and that the overall rate is quite small, $\lesssim 5$ fb, even for judicious choices of the parameters m_E, λ_E. As is well-known from past studies [38], even with well chosen cuts and with both beams polarized it will be difficult to lower the SM background to with a factor of $\sim 10-100$ times the expected signal rate for SV production in this scenario. Clearly, if S, V do decay invisibly or are very long-lived the usual search approaches for signals such as this will very likely fail.

4.2 $\gamma\gamma$ Colliders

Another way one might imagine to possibly probe the PM sector indirectly is via the process $\gamma\gamma \to VV$ in analogy to the well-studied SM $gg, \gamma\gamma \to ZZ$ reactions [39, 40] which we will briefly consider. Again, we see that this reaction is ϵ-independent with an amplitude proportional to the product $N_c(eg_D Q_{em} Q_D)^2$ for each of the PM fields circulating in the box graphs. However, like the $e^+e^- \to SV$ tree level process, this $\gamma\gamma$ reaction is, as might be expected, highly suppressed by the small values of $\sqrt{s}/m_{PM}$ that we encountered previously as we will see below.

Following the analyses as presented in Refs. [41–44], and suppressing all Lorentz indices, we note that the $\gamma\gamma \to 2V$ process in this limit can be described by the effective Lagrangian of the form

$$\mathcal{L}_{eff} = \frac{\alpha\alpha_D}{90 m_0^4}\left[\gamma_1 (F^2)(V^2) + \gamma_1' (FV)(FV) + \gamma_2 (F\tilde{F})(V\tilde{V}) + \gamma_2' (F\tilde{V})(f\tilde{V})\right], \tag{19}$$

where m_0 is a reference scale ~ 1 TeV typical of the PM masses, $F(V)$ is the photon(DP) field strength tensor and $\tilde{F}(\tilde{V})$ its corresponding dual. For fermionic and scalar PM appearing in the box graph, one finds that [41–44] $\gamma_i' = 2\gamma_i$, where the γ_i themselves are $O(1)$ sums over the various PM in the loop:

$$\gamma_i = \sum_k \eta_{(F,S),i_k} (Q_D^2 Q_{em}^2 N_c)_k \, \frac{m_0^4}{m_k^4}\,, \tag{20}$$

where the sum is over all fields in the box graph with masses m_k, *etc*, and where $\eta_{(F,S),1} = (1, 7/16)$ and $\eta_{(F,S),2} = (7/4, 1/16)$ are the relevant coefficients for (fermionic, scalar) PM fields. This leads to the $\gamma\gamma \to VV$ differential cross section in the center of mass frame, assuming that $m_{V,S}^2 << s$, of

$$\frac{d\sigma}{dz} = \left(\frac{s^3}{8\pi}\right)\left[\frac{\alpha\alpha_D}{90 m_0^4}\right]^2 (3+z^2)^2 \left[(\gamma_1 - \gamma_2)^2 + 2(\gamma_1^2 + \gamma_2^2)\right], \tag{21}$$

where $z = \cos\theta^*$ as above. Defining, similar to the above, the dimensionless ratio $y_0 = \sqrt{s}/(2m_0)$, this yields an extremely small total cross section of

$$\sigma \simeq \frac{0.29 \text{ fb}}{s \text{ (in TeV}^2)} \, \alpha_D^2 \, y_0^8 \, X\,, \tag{22}$$

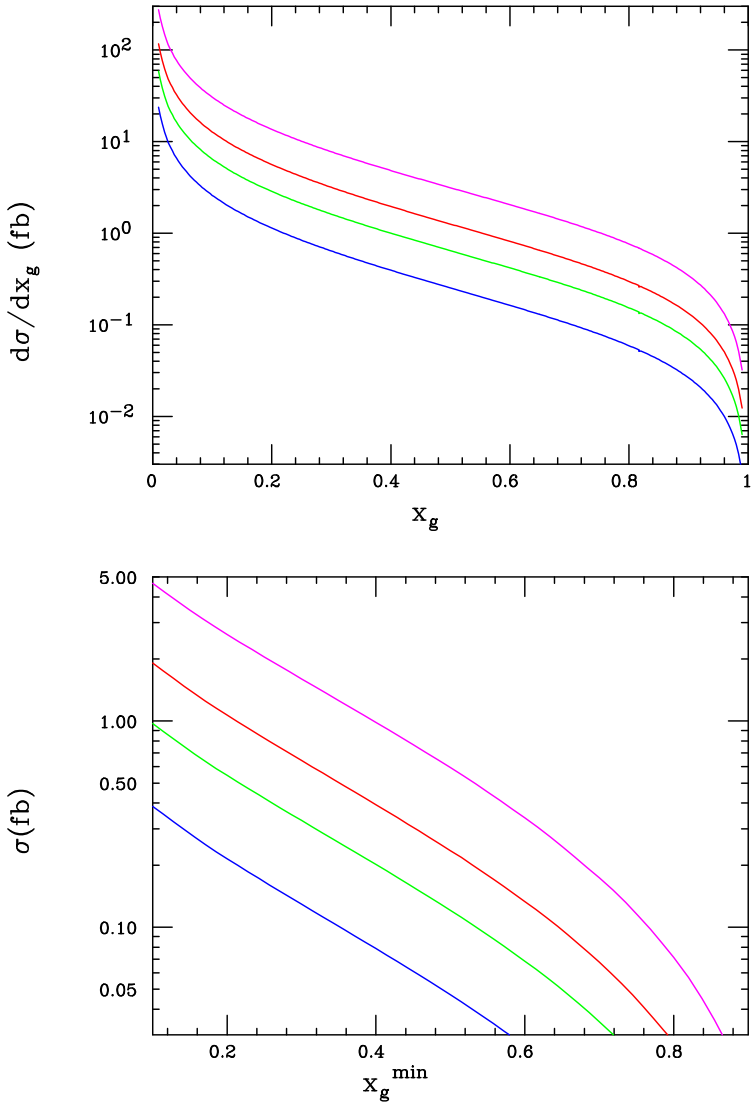

Figure 3: Emitted photon energy distribution (top) as a function of $x_g = 2E_\gamma/\sqrt{s}$ and the corresponding integrated cross section above a photon energy cut, x_g^{min}, (bottom) for the process $e^+e^- \to SV$ as described in the text assuming that $\lambda_E = 1$. From top to bottom the curves assume that $\sqrt{s} = 380$ GeV, $m_E = 1$ TeV; $\sqrt{s} = 240$ GeV, $m_E = 1$ TeV; $\sqrt{s} = 380$ GeV, $m_E = 1.5$ TeV and $\sqrt{s} = 240$ GeV, $m_E = 1.5$ TeV, respectively.

where X is the just combination of the γ_i's appearing in the final bracket in the previous expression and is expected to be $O(1)$ or perhaps slightly larger. Forgetting the effects of the photon energy distributions relevant for the $\gamma\gamma$ collider for now, by taking the suggestive values $\sqrt{s} = 0.2$ TeV, $\alpha_D = X = 1$ and $y_0 = 0.1$, we find that $\sigma = 7.3 \cdot 10^{-5}$ ab, which is essentially invisible at any foreseeable collider luminosity. Outside of some radical developments it's clear that we can forget about this particular possibility for now. However, other related $\gamma\gamma$ processes [45] may lead to somewhat enhanced production cross sections in comparison to the one we have just obtained.

4.3 LHC and HL-LHC

The most obvious new channels at the LHC (and future hadron colliders) are the production of the PM fields themselves along with any of the new gauge bosons associated with an extended dark gauge group. In almost all cases, the cross sections for the various processes we consider below can be found in Ref. [4] and which we heavily quote below.

Clearly, we need to begin this discussion by considering $\bar{D}D$ production via QCD (under the usual assumptions) and $\bar{E}E$ production via SM γ, Z exchange; these cross sections are well-known as they are identical to those for the conventionally examined vector-like quarks and leptons. For example, Fig. 2 (left) in Ref. [27] shows the total $\bar{E}E$ production cross section for both the isosinglet and, the somewhat larger, isodoublet PM cases. In the isodoublet case, the process $\bar{q}q \to W^{\pm} \to \bar{N}E + \bar{E}N$ can also occur with $m_N = m_E$, up to small mixing and radiative corrections, and with a somewhat larger cross section at the LHC as is shown in the top panel of Fig. 4 from Ref. [4]. The lower panel of this Figure also shows the total $\bar{D}D$ cross section at the $\sqrt{s} = 14$ TeV LHC from this same paper. As noted above, the signatures associated with the production of the PM states at colliders is dependent upon whether or not the DP decays invisibly, either due to a very long lifetime or via a kinematically allowed decay into DM. In the case of invisible decays, SUSY searches for sleptons and squarks can be recast to obtain the corresponding limits on PM fermions. In the case of a pair of isosinglet PM leptons decaying into e or μ pairs plus MET, this analysis has been performed in Ref. [26] for the $\sqrt{s} = 13$ TeV LHC with $\mathcal{L} = 139$ fb^{-1} leading to a lower bound of 895 GeV with a limit which is expected to be $\simeq 180$ GeV greater in the isodoublet case due to the larger production cross section [27] resulting from the alternate couplings to the SM Z. Somewhat weaker results would be expected in the case of the τ final state due to a smaller τ ID efficiency [29, 30]. A similar analysis for the $W^{\pm}$-initiated $e^{\pm}$+MET final state, as would occur for $\bar{N}E + \bar{E}N$ production, has not yet been performed. Corresponding analyses for color-triplet PM point to limits in the range of $\simeq 1.3 - 1.5$ TeV or so depending somewhat upon the the quark flavor in the final state [3, 5]. In the cases where the *very* highly boosted ($\gamma > 10^3$) DP decays visibly in the detector to lepton-jets [3] the analyses have not yet been performed but are expected to yield comparable limits but which are more strongly dependent on the model parameters and other details.

It is interesting to note that $\bar{D}D$ production at hadron colliders can, in fact, be altered in scenarios similar to the ones we have consider in the previous Section in a way not experienced by ordinary vector-like quarks. For example, in the E_6-inspired case, although the $gg, \bar{u}u, \bar{c}c \to \bar{D}D$ processes are unaffected, $\bar{d}d, \bar{s}s, \bar{b}b \to \bar{D}D$ may be modified by $t-$channel exchanges of light dark Higgs fields and longitudinal DP's due to the couplings seen above in Eqs.(5) and (6), especially so if these λ couplings are sufficiently large. Since it is easily imagined that $\lambda_i \sim g_s$, the QCD coupling, these exchanges may make substantial alterations to both the angular distributions for $\bar{D}D$ production, pushing it more forward, as well as to the overall total cross section, influencing search sensitivities, especially when the coupling is to the first generation quarks. These issues are briefly examined in Ref. [4] but a detailed study of this possibility is certainly warranted.

Finally, before moving on to the signatures of the extended gauge sector of the $2_I 1_{I'}$ scenario, one might consider the possibility of single production of the PM D state via its mixing with the $q = d, s$ or$b$ quarks. In the usual picture of single VL quark production via a SM W charged-current interaction, this process will have a cross section which sensitively dependent upon the relevant mixing matrix element. Unlike the direct Yukawa couplings of the form $\bar{q}D(G_V, S)$ discussed above, where the action of the Goldstone theorem rescues us from a possible extremely mixing suppressed interaction as we will shortly see, this salvatory effect is absent for this mechanism of single D production so that this cross section is

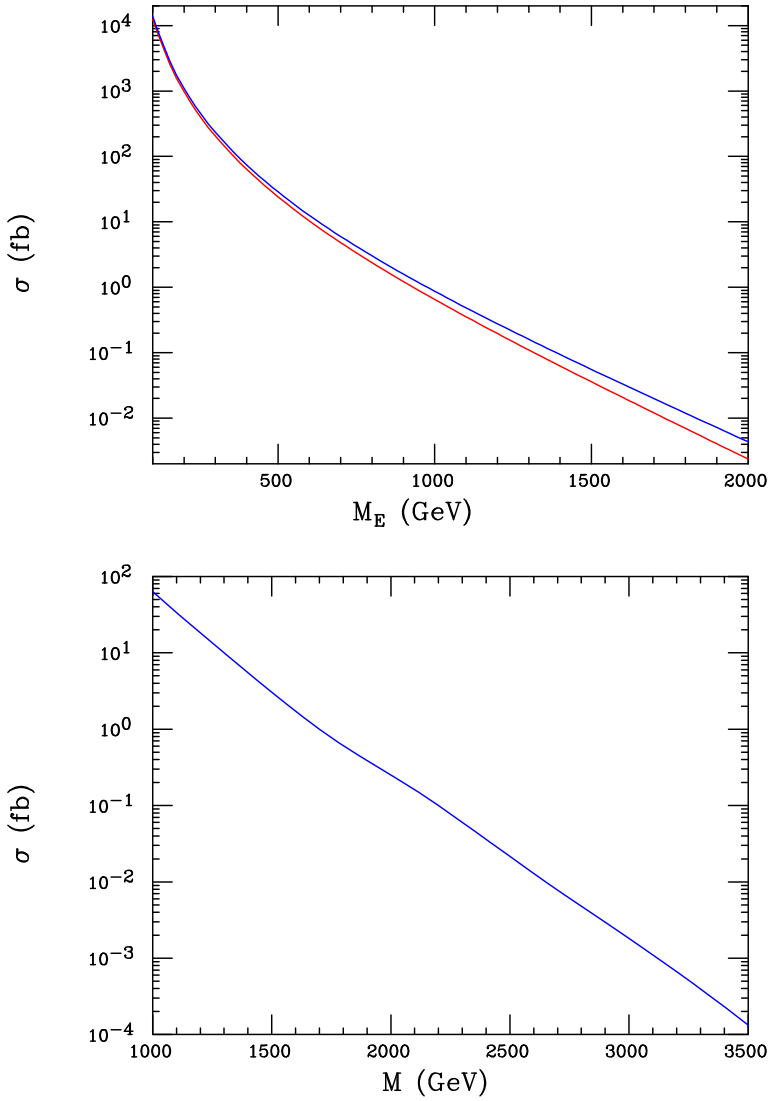

Figure 4: (Top) $q\bar{q} \to W^{\pm *}_{SM} \to E\bar{N} + N\bar{E}$ production cross section at the $\sqrt{s} = 13$ (red) and 14 (blue) LHC as a function of $m_N = m_E$. (Bottom) Inclusive QCD NNLO $\bar{D}D$ production cross section at the $\sqrt{s} = 14$ TeV LHC as a function of m_D using HATHOR following Ref. [46].

indeed quite highly suppressed. However, the $gd(s,b) \to D(S,G_V)$ associated production process cross section can indeed be quite significant, dependent only upon the values of λ_D and m_D as well as the choice of generation with which quark D is partnered within the $SU(2)_I$ doublet. We note that the enhancement seen here is similar to that observed for the decay $D \to qG_V$ in comparison to, *e.g.*, $D \to Zq$ that was discussed above. The $gq \to DG_V$ sub-process differential cross section for this reaction employing the same notation as above is given in the limit that $m^2_{V,S} << \hat{s}$ by

$$\frac{d\sigma}{dz} = \frac{\alpha_s \lambda_D^2}{16\hat{s}} \left[\frac{\hat{s}}{-t} + \frac{-t}{\hat{s}} - 2 - 2m_D^2 \left(1 + \frac{m_D^2}{t}\right)\left(\frac{1}{t} + \frac{1}{\hat{s}}\right)\right], \tag{23}$$

where $\hat{s}$ is the the sub-process center of mass energy squared as usual and where $t = \frac{-\hat{s}}{2}(\tilde{E} - \tilde{p}z)$ with $\tilde{E}, \tilde{p} = 1 \pm \frac{m_D^2}{\hat{s}}$, respectively. Fig. 5 shows the total cross section for this process at the $\sqrt{s} = 13$ and 14 TeV LHC as a function of m_D assuming that $\lambda_D = 1$ for ease of rescaling. Here we see that, indeed, at smaller values of m_D (again, for $\lambda_D = 1$), this cross section is quite comparable to the familiar $\bar{D}D$ cross section (when $q = d$), this being enhanced by the larger gluon parton density while simultaneously being suppressed by the relative heavy D phase space. For larger values of m_D, this associated production process may yield a larger rate when $q = d$. Of course, for $q = s, b$, the cross section for all values of m_D is seen to be somewhat smaller as would be expected. Assuming that S/V produces MET as discussed above, the experimental constraints from a lack of any monojet signature at the LHC can be used to place constraints in the $\lambda_D - m_D$ parameter plane for the different choices of q; this analysis has yet to be performed.

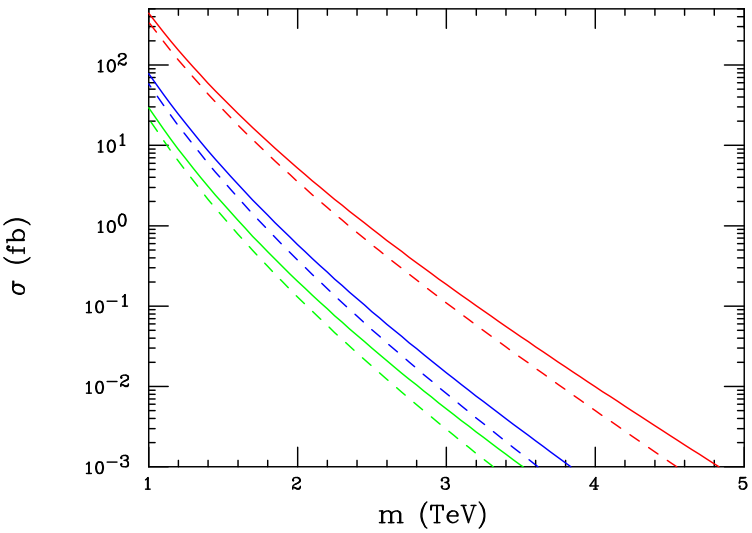

Figure 5: The $gq \to D(G_V, S)$ production cross section at the $\sqrt{s} = 14$(solid) and 13(dashed) TeV LHC in the Goldstone Boson Approximation as a function of the mass of the D assuming that $\lambda_D = 1$. From top to bottom, the curves are for $q = d, s, b$, respectively.

We now turn to the production of the new gauge bosons present in this model. The production of and signatures for the $Q_{em} = Q_D = 0$, E_6-inspired gauge boson, Z_I, are in many ways similar to a host of familiar Z' scenarios [31, 47–49] but with some potentially very interesting differences depending upon the PM mass spectrum, its flavor nature, as well as the value of the parameter x_I which appears in its couplings and controls the $Z_I - W_I$ mass relationship, *i.e.*, if $x_I > 3/4$ the decay $Z_I \to W_I W_I^\dagger$ can occur on-shell due to the usual non-abelian coupling. Recall that Z_I couples to the familiar-looking combination $\frac{g_I}{c_I}(T_{3I} - x_I Q_D)$ so that the T_{3I} assignments of the SM fermions and PM fields will play an

important role in its phenomenology. Note that in all cases, the Z_I does *not* couple to the u, c, t quarks. It is at this point where the question of whether only a single SM generation (and indeed *which* one) or all three generations have PM partners and thus carry $SU(2)_I$ quantum numbers perhaps becomes the most critical. For example, if Z_I only couples to the second generation of the SM, then it can only be produced via $\bar{s}s$ annihilation and decay to the unique charged lepton $\mu^+\mu^-$ final state. This is also directly related to the question of how, *e.g.*, D mixes with d, s, or b or whether there is a D for each generation. To cover all these possibilities, we consider two extreme cases: one where only a single specific generation is augmented by PM fields (which has important flavor physics implications) or instead, where all three of the SM generations are augmented and so that the usual family universality is enforced.

Perhaps the simplest possible scenario is where the Z_I can decay only to SM particles by kinematic constraints, *i.e.*, $m_{Z_I} < 2m_{PM}, 2m_{W_I}$. Since the SM fields by definition have $Q_D = Q_I = 0$, the Drell-Yan signal rate for $\bar{q}q \to Z_I \to \ell^+\ell^-$, in the narrow-width approximation (NWA), σB_ℓ, with B_ℓ being the leptonic branching fraction for $Z_I \to \ell^+\ell^-$, is independent of x_I but does depend upon the overall coupling strength g_I/c_I which is unknown *a priori*. Writing $g_I/c_I = r\ g/c_w$, σB_ℓ is then totally determined up to an overall factor of r^2 as a function of m_{Z_I} since only SM final states are involved. Here we will assume that $r = 1$ so that our results can easily be appropriately rescaled by this overall factor. The first case we will consider is that where all 3 SM generations carry $2_I 1_{I'}$ quantum numbers, *i.e.*, generation-independence/family universality exists as is typically the case in Z' models with the results shown in Figs. 6 and 8 from Ref. [4]. As can be seen here, the present ATLAS null searches [50] employing 139 fb^{-1} of $\sqrt{s}$ =13 TeV integrated luminosity presently excludes Z_I masses below $\simeq$ 5.2 TeV under these set of assumptions. A similar null search performed at the $\sqrt{s}$ =14 TeV HL-LHC with 3 ab^{-1} of luminosity [51] would increase the exclusion limit on a Z_I to masses $\simeq$ 5.9 TeV [4] under the same set of assumptions.

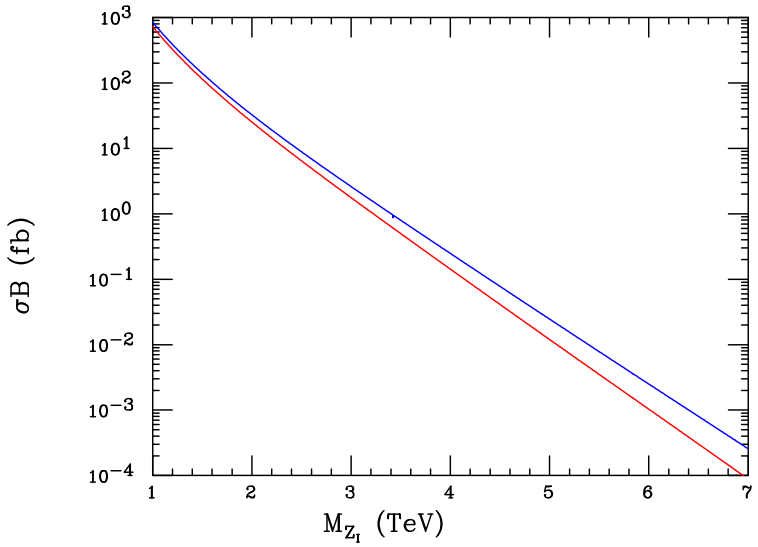

Figure 6: The values of σB_ℓ for Z_I production as a function of mass at the $\sqrt{s} = 13$ (red) and 14 (blue) TeV LHC. Here, only decays to SM fields are assumed to be kinematically allowed and $r = 1$ is assumed. It is assumed here that the Z_I couples in a generation-independent manner.

The next logical case is where only a single SM generation carries non-trivial values of T_{3I} and so couples to the Z_I. While the value of B_ℓ is the same in all three case (being a factor of 3 larger than in the universal case just discussed), the production cross section itself is not as the $\bar{d}d$, $\bar{s}s$ and $\bar{b}b$ parton luminosities are all very different. Fig. 7 from [4] shows the values of σB_ℓ in these three individual cases, here ignoring any effects from inter-generational mixing for simplicity.

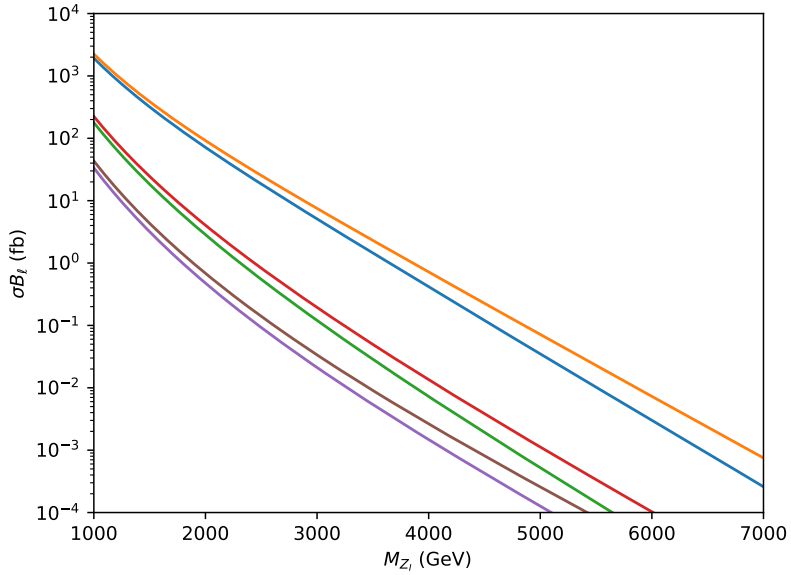

Figure 7: σB_ℓ for Z_I production at the $\sqrt{s} = 13$ (lower) and 14 TeV (upper) LHC as a function of mass with $r = 1$. For each pair of curves it is assumed that the Z_I only couples to a single SM generation and that decays to PM and W_I are kinematically forbidden. From top to bottom, the curves correspond to a Z_I coupling to the first, second, or third generation of the SM, respectively, in the absence of mixing.

Fig. 8 from Ref. [4] then shows how these Z_I production cross sections in the various dilepton channels translate into current LHC search limits and the expectations for the HL-LHC assuming either universal couplings or coupling to only one of the SM generations. In order to obtain these results in the case of the $\tau^+\tau^-$ third generation couplings, the results from an ATLAS $b\bar{b} \to H \to \tau^+\tau^-$ study [52, 53] were recast, making corrections for the detector acceptance differences between spin-0 and spin-1 resonances.

As far as the Drell-Yan signal channel is concerned the final layer of complexity arises when decays into the PM and other exotic fermions as well as W_I pairs (when $x_I > 3/4$) are kinematically accessible. In the NWA, this has no effect on the the Z_I production cross section itself but leads to a suppression of B_ℓ as other decay channels are now open. To be specific, let us consider the generation-independent cases and ask how this suppression of B_ℓ can depend upon the value of x_I; recall that $m^2_{W_I} = (1 - x_I)\, m^2_{Z_I}$ is fixed but that the PM and other exotic particle masses relative to m_{Z_I} are unknown. For simplicity, we will here assume that all of the PM fields have a common mass value. Figure 9 from Ref. [4] shows the resulting suppression of B_ℓ as a function of x_I under these assumptions. It is seen that the impact of these additional decay modes will not have a huge effect on the Z_I signal rate expected.

Unlike the W' of, *e.g.*, the familiar Left-Right Symmetric model [54], the *neutral* - but non-hermitian - $W_I^{(\dagger)}$ has $Q_{em} = 0$ but now carries $Q_D = \pm 1$ so cannot be singly produced in the absence of the fermion mixing that is induced by $U(1)_D$ breaking and so is very highly suppressed by factors of order $v^2_{1,4}/v^2_3 << 1$. This implies that we must instead examine the pair- and/or associated-production channels, *e.g.*, $W_I W_I^\dagger$, $W_I^\dagger + D + h.c.$, *etc*, that conserve Q_D to lowest order. While $W_I W_I^\dagger$ production proceeds via Z_I and D exchange, associated production occurs via the process $g(d, s, b) \to W_I^\dagger + D + h.c.$. Both of the rates for these processes will clearly depend upon whether only a single generation of PM exists or if there are PM partners for each generation. Interestingly, when $x_I > 3/4$ happens, resonant W_I-pair production can occur via the Z_I making for a significant rate enhancement; in either case these are both interesting production mechanisms to consider. Due to the Goldstone Theorem, a third process is also possible, *e.g.*,

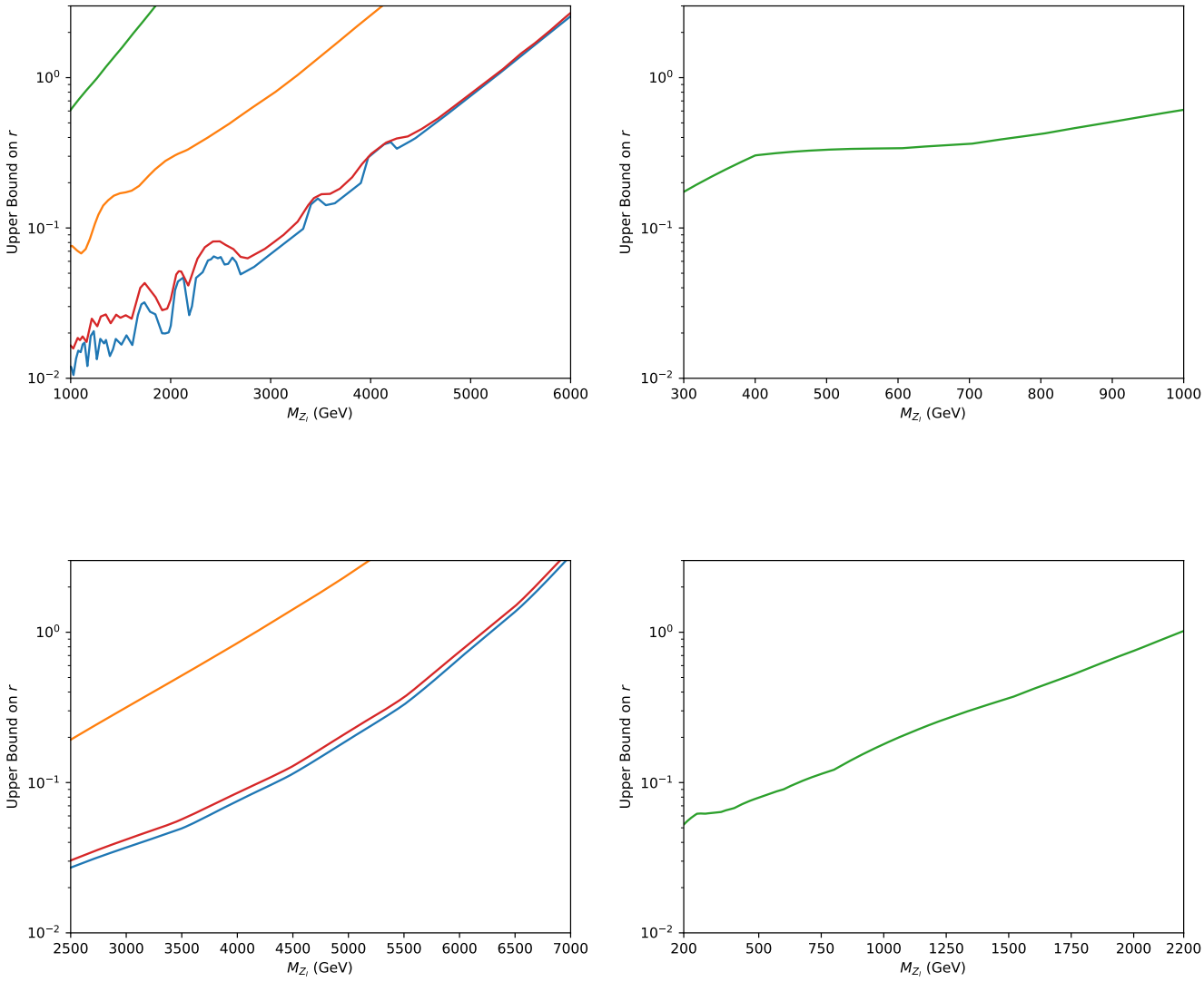

Figure 8: (Top Left) Limits from the $\sqrt{s} = 13$ TeV LHC on the values of the parameter r as described in the text, as a function of the mass of the Z_I, employing the results from ATLAS searching for dilepton decays [50, 52]. From left to right the curves correspond to only third generation couplings (green), only second generation couplings (gold), universal couplings (red), and only first generation couplings (blue). (Top Right) Extrapolation of the results in the previous panel for the case of third generation couplings to lower Z_I masses. (Bottom Left) Same as the top left panel, but now employing an ATLAS analysis assuming a null result at the HL-LHC with $\sqrt{s} = 14$ TeV and L=3 ab^{-1} [51]. (Bottom Right) The corresponding limit in the $\tau^+\tau^-$ case employing the ATLAS heavy Higgs study [53] with acceptance corrections included for a spin-1 state.

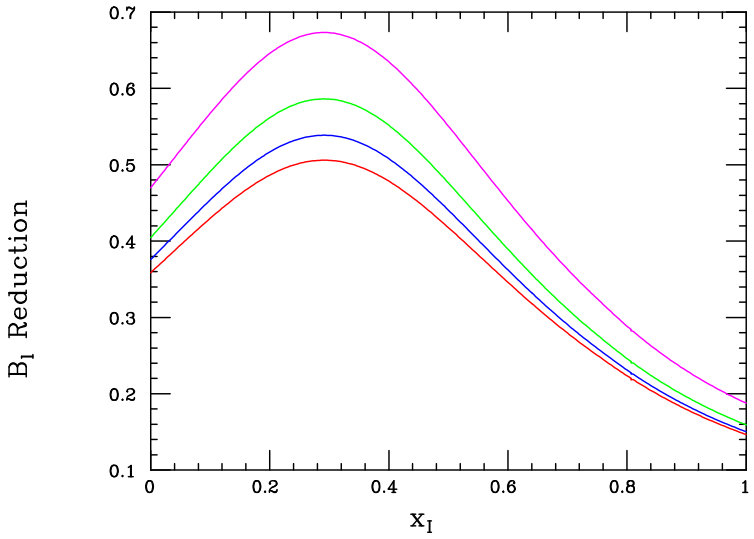

Figure 9: Multiplicative B_ℓ suppression factor for the Z_I as a function of x_I due to the additional non-SM decays into 3 generations of degenerate exotic/PM fermions plus $W_I W_I^\dagger$ (for $x_I > 0.75$) as discussed in the text. From bottom to top the curves assume a common value of $m_{PM}/m_{Z_I} = 0, 0.2, 0.3$ and 0.4, respectively.

$\bar{d}d \to W_I + V/S + h.c.$, and similarly for $d \to s, b$, but with suppressed rates due to the differing parton luminosities. We will examine each of these mechanisms in turn. Note that the associated production process is similar in nature to the $gd(s,b) \to DV_L$ process examined above.

We note that there will always be an *indirect* bound on the W_I mass within this setup arising from the corresponding constraint on the Z_I mass from the previous discussion due to the mass relationship $m^2_{W_I} = (1 - x_I)m^2_{Z_I}$. Below we will concern ourselves with *direct* production constraints but this relationship and its possible impact on searches should always be kept in mind.

The cross section for the associated production process, assuming a given flavor of initial state quark, depends rather sensitively on the combined heavy D and W_I masses as well as the overall coupling, g_I^2, which we can scale to the usual SM $SU(2)_L$ gauge coupling, g, leaving an overall unknown scale factor similar to what we did above for the case of Z_I. The resulting cross sections as a function of the W_I mass for various choices of m_D are shown in Fig. 10. The two upper panels correspond to the cases where $q = d$ for $\sqrt{s} = 13$ and 14 TeV, respectively, while the lower panels are for 14 TeV with $q = s$ or b, respectively; in all cases one sees that a large part of the model parameter space is potentially kinematically accessible for all choices of q at $\sqrt{s} = 14$ TeV. Once $W_I D$ is produced, then $D \to qA_I(= V), qS$ (with $q = d, s$ or b) as discussed above and, if $m_{W_I} > m_{D,E}$, then the W_I will rapidly decay as $W_I \to Dq, Ee$ with D, E then decaying as previously described. It is to be noted that if W_I is less massive than D (or E, N, *etc*) it could possibly decay into a 3-body final state, *e.g.*, $W_I \to \bar{e}E^* \to e^+e^- + V/S$ with a consequently longish lifetime. For $W_I D$ production and hadronic W_I decay, we observe that the final state is somewhat similar to that for $\bar{D}D$ production as discussed above (which provides a significant background) but with a mandatory extra jet which, if not flavor-tagged, could be easily by mimicked by QCD ISR. Within that region of parameter space where V, S decay inside the detector so that the D's can be reconstructed, the corresponding reconstruction of the W_I mass peak using the extra q jet would then lead to a substantial reduction of the significant QCD background. This production process requires a further, more detailed study. Of course, in the case where $W_I \to \bar{e}E$, the final state will appear as a lepton plus jet combined with MET.

The $\bar{q}q \to W_I W_I^\dagger$ process for $q = d, s, b$ takes place via $s-$channel Z_I exchange as well as $t-$channel D

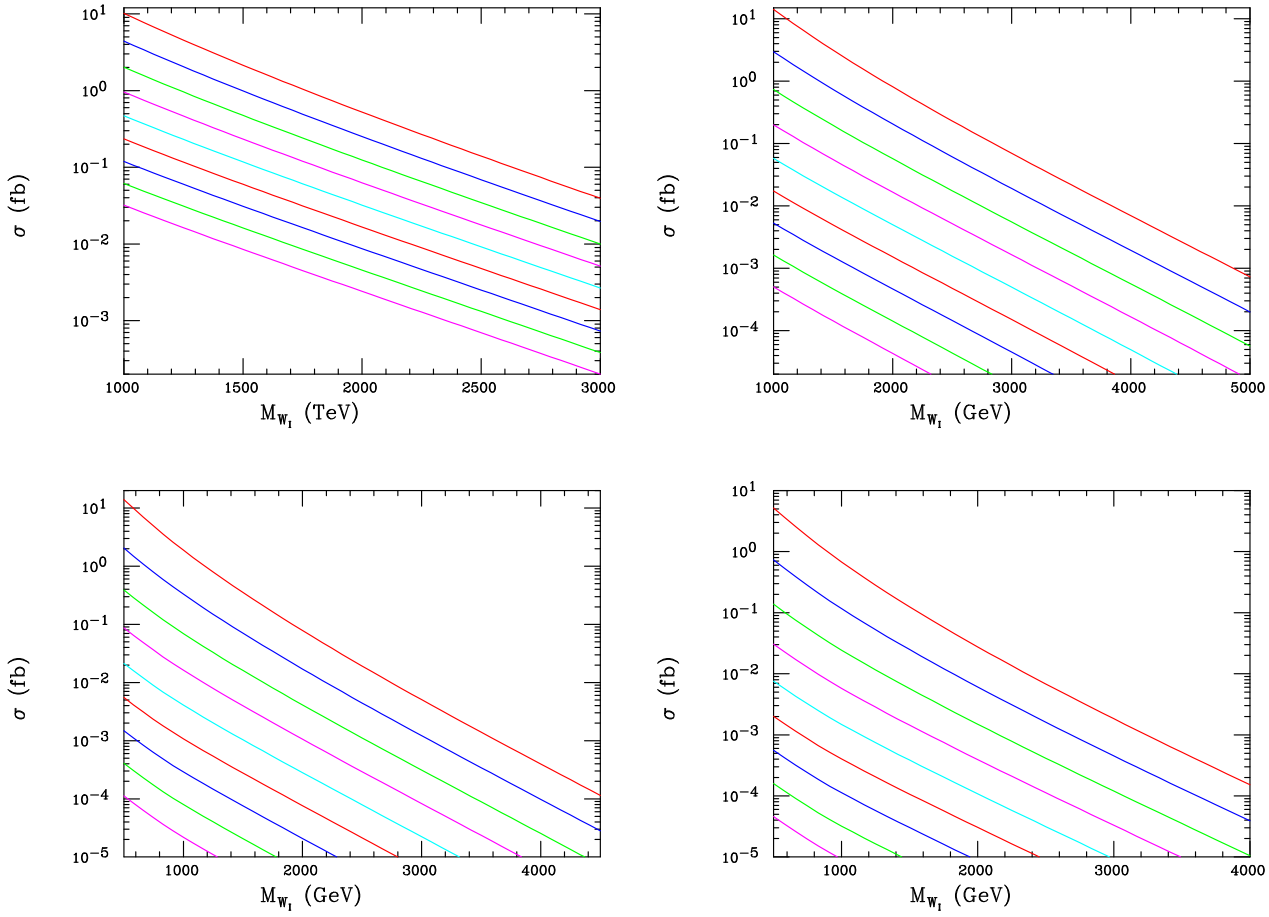

Figure 10: (Top Left) $gd \to DW_I + h.c.$ associated production cross section, taking $(g_I/g)^2 = 1$, as a function of the W_I mass assuming, from top to bottom, that $m_D = 1, 1.25, .., 3$ TeV, respectively, at the 13 TeV LHC with d being D's SM partner. (Top Right) Same as the previous panel but now for 14 TeV LHC and for $m_D = 1, 1.5, ..5$ TeV. (Bottom Left) and (Bottom Right) Same as the previous panel but now assuming $s(b)$ is the SM partner coupling to D, respectively.

exchange which destructively interfere to maintain unitarity and is similar to the case of W^+W^- production in the SM. The overall cross section will, again, be highly sensitive to the choice of q due to the parton luminosities. Recall that the W_I and Z_I masses are correlated via the familiar-looking $m_{W_I} = m_{Z_I} c_I$ relationship[4]. Due to this mass relationship, this production cross section depends upon the parameters m_{W_I}, m_D, x_I and, as an overall factor, the ratio $(g_I/g)^4$. As in the case of associated production, since a heavy W_I-pair is produced the discovery reach for W_I in this channel will be significantly reduced in comparison to the case of single, resonant Z_I production. For fixed masses (and the ratio g_I/g), as x_I increases from a small value we expect the cross section to grow as more and more as the cross section increasingly probes the effects of the Z_I resonance until on-shell resonant production becomes possible. In that case, the value of the Z_I reduced width, Γ_{Z_I}/m_{Z_I}, will also become relevant as the $W_I W_I^\dagger$ cross section will be related to height of the resonance peak, hence, the other Z_I decay modes. This reduced width, for $g_I/g \sim 1$, is expected to be roughly $\simeq 0.01 - 0.03$ based on the discussion above and we will assume this range to be the case in the analysis below. Obviously, the larger the reduced width becomes, the smaller will be the effect of the resonance enhancement on the W_I pair production cross section.

Some examples from these considerations can be found by examining the cross sections as shown in both Figs. 11 and 12 from Ref. [4]. A strong x_I-dependence is clearly observed at larger values, as we anticipated, due to the action of the Z_I resonance. Interestingly, *e.g.*, we note that with d and D sharing an $SU(2)_I$ isodoublet, assuming for purposes of demonstration, *e.g.*, $m_D = m_{W_I} = 1$ TeV, the associated production process leads to the larger of the two cross sections at $\sqrt{s} = 14$ TeV by over an order magnitude when $x_I \leq 0.7$ as might be expected from a mixed QCD-electroweak process. Of course, once Z_I resonance is substantially probed the pair-production cross section is seen to easily dominate. We also note that as the value of m_D increases, we effectively turn off the t-channel exchange and thus the resulting interference between the two contributions essentially goes away so that the cross section *rises* in the example seen in the top panel of Fig. 11. As in case the ratio m_t/m_W in the SM, we know, tree-level unitarity will impose a constraint on the ratio of these masses of roughly $m_D/m_{W_I} \lesssim 10$, depending upon the value of g_I. The sensitivity of the cross section to the reduced Z_I width is shown in the lower panel of Fig. 11 while the sensitivity to m_{W_I} for fixed $x_I = 0.25$ for different choices of $q = d, s, b$ is shown in Fig. 12.

The signatures here, as was in the case of $W_I D$ associated production, will depend on the kinematically allowed decay modes of the W_I. As observed above, these are rather straightforward so long as, generically, $m_{W_I} > m_{PM}$ so that a rapid tree-level decay is allowed. As noted, when this is *not* the case, the W_I may be potentially relatively long-lived as only off-shell decays via PM will be allowed, *e.g.*, $W_I \to eE^* \to e^+e^-V$. If W_I can decay to both E and D final states, interesting mixed signatures of lepton+jets+MET type can arise from W_I pair production.

The $2_I 1_{I'}$ gauge structure also allows for the $\bar{q}q \to W_I V/S + h.c.$ production mechanism for $q = d, s, b$ via $t-$channel D exchange with a rate scaling as $(g_I\lambda)^2$ [4]. For λ's which are $O(1)$ as is expected, this single W_I production process can be advantageous since only a single heavy particle appears in the final state and so has an edge kinematically over both $W_I W_I^\dagger$ and the $W_I D$ mechanisms. Cross sections for this reaction are shown in the top panel of Fig. 13 as functions of m_{W_I} for the three different choices of q and various values of m_D. Here we do indeed see larger production rates for at least part of the parameter space yet associated production remains competitive due the larger gluon parton density and the partial QCD associated production mechanism.

Finally, in analogy to the previously examined $e^+e^- \to 2V, 2S, VS$ set of processes discussed above, the corresponding $\bar{q}q$-initiated processes for $q = d, s, b$ can be probed at the LHC but now taking place now via D exchange in the $t-$ and $u-$channels. The cross sections in this case will, of course, now scale as λ_D^4 as is shown in the lower two panels of Fig. 13. Here, apart from an overall factor of λ_D^4, the two relevant cross sections depend only upon the value of m_D and the choice of $q = d, s, b$. As we observed in the case of the e^+e^- initial state, the equal $2V$ and $2S$ cross sections are suppressed relative to that for VS due to the destructive interference of the $t-$ and $u-$channel amplitudes. However, in the likely case that S, V are either long-lived or decay to DM particles, this final state alone will be invisible, so, in analogy with the e^+e^- case, we use QCD ISR to act as a trigger and then search for jets plus MET final

[4]Also recall that $c_I^2 = 1 - x_I$ and that the on-shell decay $Z_I \to W_I W_I^\dagger$ becomes kinematically allowed when $x_I > 3/4$.

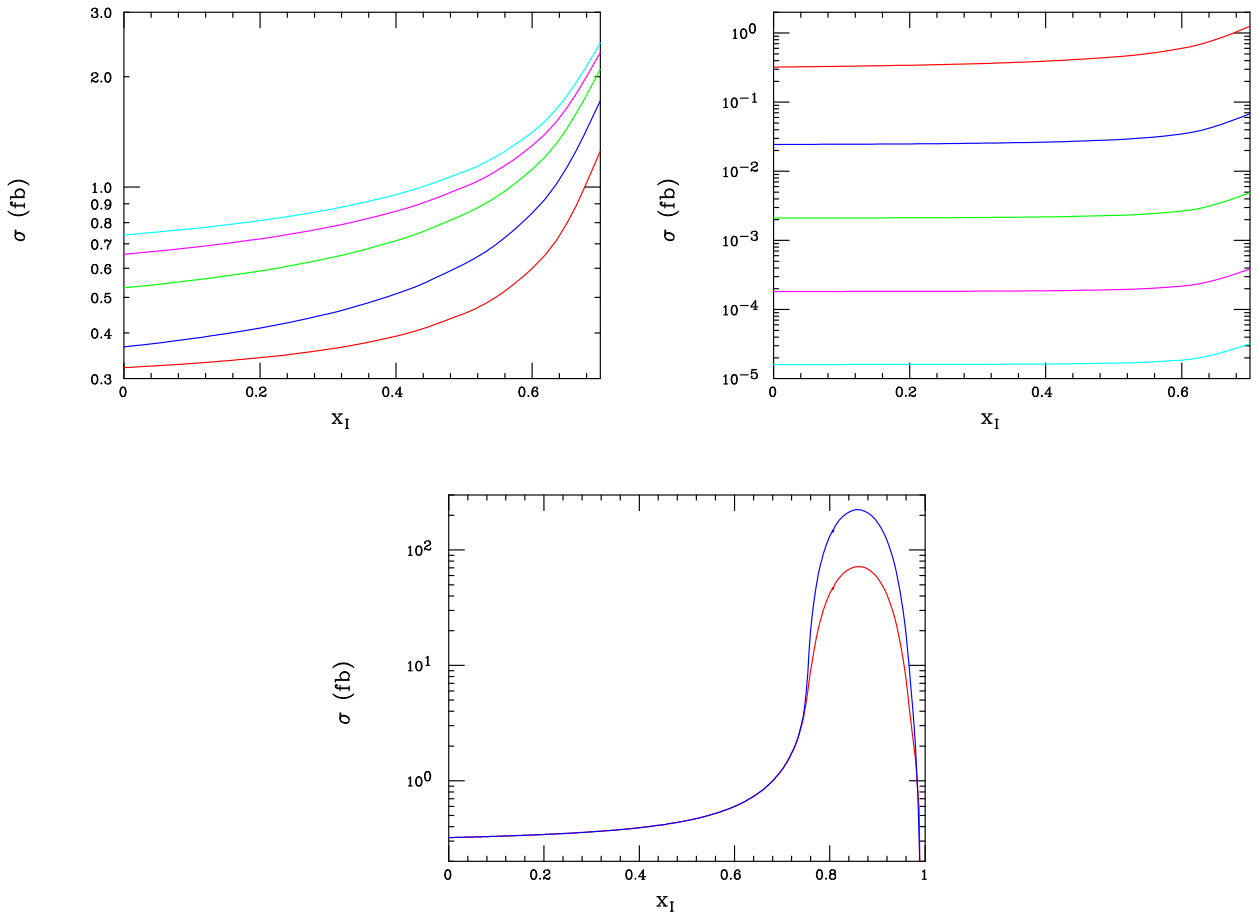

Figure 11: (Top Left) $q\bar{q} \to W_I W_I^\dagger$ total cross section at the $\sqrt{s} = 14$ TeV LHC as a function of $x_I = s_I^2$ assuming $M_{W_I} = 1$ TeV and, from bottom to top $m_D = 1, 2, .., 5$ TeV, respectively, with d being D's SM partner. Here an overall scaling by $(g_I/g)^4$ is still required as in the case of associated production. (Top Right) Same as the previous panel but now with $m_D = 1$ TeV and, from top to bottom, $m_{W_I} = 1, 1.5, .., 3$ TeV, respectively. (Bottom) Same as the previous panel but now assuming that $m_{W_I} = m_D = 1$ TeV and including the Z_I resonance region at large x_I assuming that $\Gamma_{Z_I}/m_{Z_I} = 0.01(0.03)$ as the top blue(bottom red) curve.

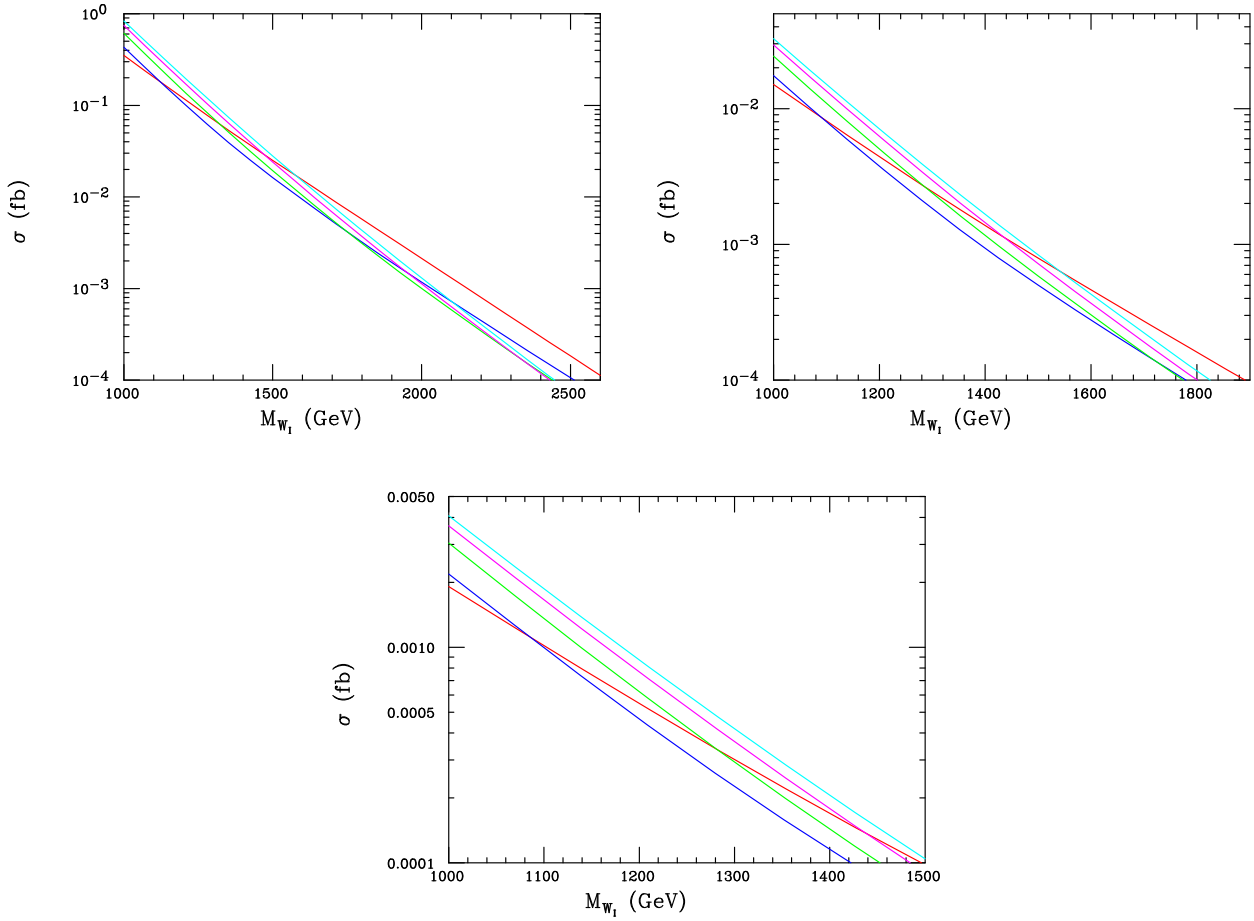

Figure 12: (Top Left) Same as the in the previous Figure but now assuming that $x_I = 0.25$ and displayed as a function of m_{W_I} with, from bottom to top at the left axis, $m_D = 1, 2, .., 5$ TeV. (Top Right, Bottom) Same as the previous panel but now assuming $s(b)$ is the SM partner to D in the $SU(2)_I$ doublet, respectively.

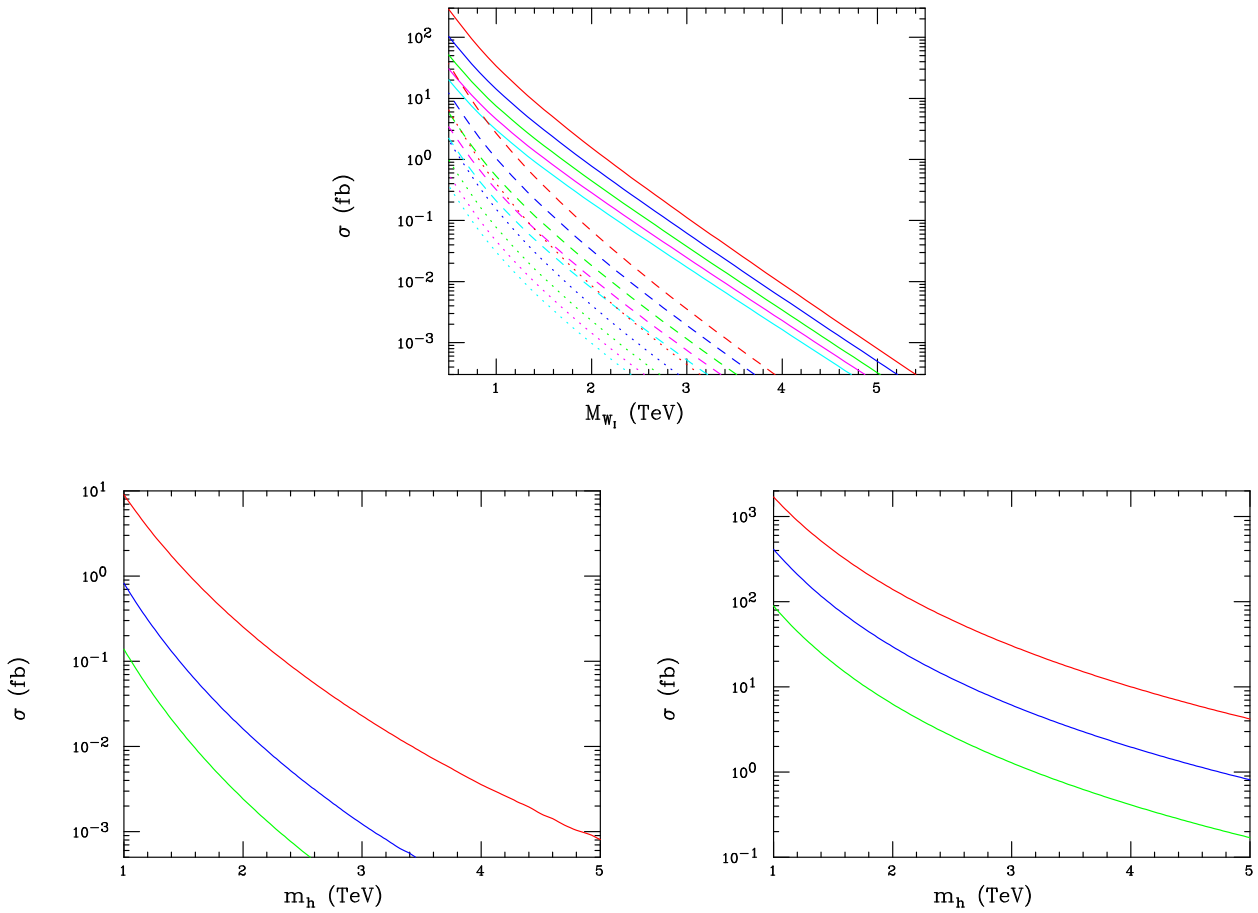

Figure 13: (Top) The $W_I^{(\dagger)}V/S$ associated production cross section as a function of m_{W_I} and in units of $(g_I\lambda_D/g)^2$ at the $\sqrt{s} = 14$ TeV LHC. Here the curves are for the choice of $d\bar{d}$ (solid), $s\bar{s}$ (dashed) or $b\bar{b}$ (dotted) initial states assuming, from top to bottom in each set, that $m_h = m_D = 1,..,5$ TeV, respectively. (Bottom Left) V or S pair production cross section in units of λ^4 as a function of $m_h = m_D$ assuming, from top to bottom, $q = d, s, b$, respectively. (Bottom Right) VS associated production cross section in units of λ^4 as a function of $m_h = m_D$ assuming, from top to bottom, $q = d, s, b$, respectively.

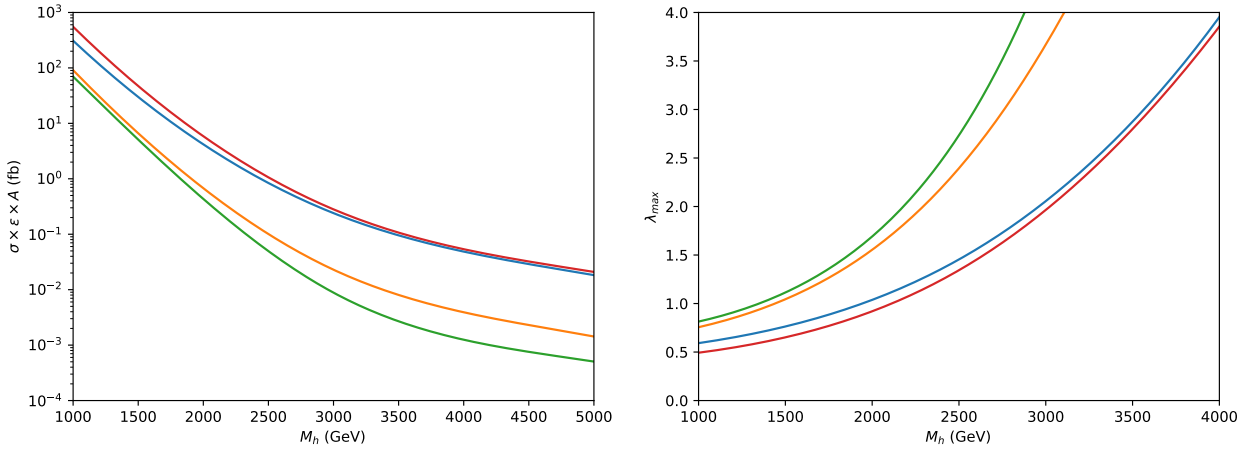

Figure 14: (Left) The signal cross section $\sigma \times \epsilon \times A$ in the ATLAS IM1 search region [55] for $pp \to 2V, 2S, VS + 1 - 4j$ as a function of $m_h = m_D$ up to an overall factor of λ_D^4 at the $\sqrt{s} = 13$ TeV LHC. IM1 corresponds to $E_T^{miss} > 250$ GeV in addition to the cuts on jets and leptons described in detail in Ref. [4]. The red (blue, gold, green) line corresponds to D coupling equally/universally to all generations (only d, only s, only b). As m_D increases, the case of universal couplings becomes increasingly dominated by the first generation. (Right) Upper bounds on λ_D from the monojet search of Ref. [55]. As m_D increases, the case of universal couplings is dominated by the first generation result and the upper bounds on λ_D converge.

states. However, we can go further and allow for gq and/or gg initial states that will yield additional hard jets as part of the overall production process. This analysis was performed in detail in Ref. [4] (to which we refer the interested Reader) and then compared in detail with the monojet results obtained by ATLAS in Ref. [55] for a number of distinct signal regions resulting in the constraints as shown in Fig. 14. The ATLAS IM1 signal region essentially always provided the tightest set of constraints yielding the upper limit on λ as a function of m_D (denoted by m_h here) as shown in the right panel of this Figure.

5 Scalar PM

So far we have concentrated on the case where the PM fields are dominantly fermionic in the previous Sections although they are just as likely to be, *e.g.*, color-singlet scalars as was mentioned above. In a bottom-up approach, as in the earlier fermionic toy models first discussed above, we seek an addition to the SM scalar spectrum that allows for PM instability, generates a finite and calculable value for ϵ as well as having a means to break the $U(1)_D$ symmetry. These constraints are rather non-trivial. If we add only a pair of, *e.g.*, $Q_{em} = 1, Q_D = \pm 1$ scalars, ϕ_i^+, similar to the E_i above, we can mix them with the SM Higgs doublet so that they can decay and ϵ will be finite; however, $U(1)_D$ will remain unbroken. If these were instead neutral scalars so that they could obtain $U(1)_D$-breaking vevs, then $\epsilon = 0$. Clearly some combination of charged and neutral scalars carrying $Q_D \neq 0$ need to be added to satisfy our goals. Given this, as shown in Ref. [6] which we closely follow here, it is easy to convince oneself that the simplest possibility simultaneously satisfying all the model building constraints is to add two additional $SU(2)_L$ isodoublet Higgs representations, $\eta_{1,2}$, to the SM that have $Q_D = \pm 1$, respectively, but whose neutral members also obtains the small vevs, $v_i \leq 1$ GeV (with $t = v_1/v_2$ so that we can take ≥ 1 without loss of generality), that are necessary to break $U(1)_D$. In such a case these new doublets act not only as PM but as the source of the Higgs fields in the dark sector. In the case of more complex scalar sectors with multiple new fields, however, it is possible to separate these two roles so that the scalars with $U(1)_D$ breaking vevs and those that circulate in the $U(1)_Y - U(1)_D$ vacuum polarization-like graphs are distinct. Here we will focus on this simpler scenario which is quite highly constrained for numerous reasons: the

$U(1)_D$ breaking vevs must be small, $\lesssim 1$ GeV, the Higgs potential must be bounded from below, the various unitarity, electroweak and Higgs(125) coupling constraints must all be satisfied, as must also be the bounds from the non-observation of new, heavier scalar states at the LHC. Additional constraints are obtained from measurements/bounds on the invisible decay widths of the SM Z, which is proportional to $t^2 - 1$ (thus forcing the value of t to be not too far above unity), as well as those from the 125 GeV SM-like Higgs. Although this model has many free parameters because of the complexities of the scalar potential, it is quite likely that due to these numerous constraints this scenario will either be realized or excluded once an additional rather small amount of integrated luminosity at $\sqrt{s} = 14$ TeV is accumulated by the LHC.

As discussed in detail in Ref. [6], after spontaneous symmetry breaking, in the limit of a CP-conserving scalar potential with real vevs, the physical scalar spectrum will consist of the (almost) SM Higgs, h_{SM} with $m_{h_{SM}} \simeq 125$ GeV, two pair of charged Higgs, $H^{\pm}_{1,2}$ [5], one CP-odd state, A (the remaining ones playing the roles of the SM and $U(1)_D$ Goldstone bosons), as well as two additional CP-even states, one of which is heavy and close in mass to the CP-odd state (A), H, and one of which is quite light with a mass $\lesssim 1$ GeV that we can identify with the dark Higgs, $h_d = S$, in the discussion above. The size of the mixing between the SM Higgs and the other CP-even states in $\eta_{1,2}$ is quite small as $v^2_{1,2}/v^2_{SM} \sim 10^{-4} \sim \epsilon$. Due to the various small parameter ratios it is easy to diagonalize the scalar mass matrices and rewrite the 14 parameter Higgs potential [6] in terms of eigenstate masses (which are required to be positive definite), $v_{SM}, t, v^2 = v_1^2 + v_2$ and ϵ plus some additional parameters. As in the E_6-inspired model above, the DP in this scenario also picks up a coupling proportional to those of the SM Z since the dark Higgs fields are both in $SU(2)_L$ isodoublets. Since the charged Higgs act as the only PM in the vacuum polarization loop, we can immediately see that ϵ is indeed finite, calculable (and can be of either sign) and is given by

$$\epsilon = \frac{g_D e}{48\pi^2} \ln\left(\frac{m_2^2}{m_1^2}\right), \tag{24}$$

with m_i being the mass of $H_i^{\pm}$ and is of the expected magnitude, $|\epsilon| \lesssim 3 \times 10^{-4}$; recall the values of $m_{1,2}$ are *not* mass ordered here. It is important to note that in the absence of $U(1)_D$ breaking, gauge invariance prevents any of these new Higgs states from coupling to the SM fermions and so these interactions are suppressed by factors of order v_i/v_{SM} and can generally be safely neglected in comparison to usual gauge interactions in practice.

Perhaps the best way to examine this rather large parameter space is via a Monte Carlo scan [6], randomly generating points with it, requiring that all of the many constraints discussed above (apart from those from the LHC specifically to be discussed below) are satisfied simultaneously and then study those points which survive. As part of this scan, it was also required that $m_A > 120$ GeV and $m_{1,2} > 200$ GeV as the spectrum tends to be rather light and such light states would likely be rather easily excluded by LHC searches. A sample of $\simeq$7k points survive this scan which we make use of below. An idea of the mass spectra that are possible in this scenario after the constraints are applied can be gleaned from Fig. 15 where we see that *both* charged Higgs states must lie below $\simeq 420$ GeV, both only partially concentrated in the lower mass range, while we also observe that $m_A \simeq m_H \lesssim 200$ GeV with, again, smaller masses preferred. Combinations of the new heavy scalars can be produced at the LHC via their SM gauge interactions with the $W^{\pm}$, γ and Z via s-channel gauge boson exchanges as we will make use of below.

Once produced, the decays of these new heavy scalars provide for discovery signatures at the LHC. Note that since they do *not* couple to the SM fermions at leading order, many of the typical searches performed at the LHC for heavy scalars, *e.g.*, in the Two Higgs Doublet Model, do not apply to this scenario. Both charged Higgs will decay as $H_i^{\pm} \to W^{\pm} h_d/V$ with equal rates and to $W^{\pm}H/A$, also with equal rates, if kinematically allowed. The heavy CP-even state, H, will decay to either ZV or to $h_{SM}h_d$ while we find that $\Gamma(A \to h_{SM}V) \simeq \Gamma(H \to h_{SM}h_d)$ and $\Gamma(A \to Zh_d) \simeq \Gamma(H \to ZV)$, essentially due to the Goldstone Theorem. Clearly, the ratio of partial widths, $R = \Gamma(H \to ZV)/\Gamma(H \to h_{SM}h_d)$, then determines which decay mode is dominant and thus what final states should be searched for at colliders. Fig. 16 shows this ratio R as a function of m_H for the $\simeq$ 7k model points, and we find that for $\simeq 72\%$

[5] Note that $H_i^{\pm}$ arises from the doublet η_i so that they are *not* mass ordered

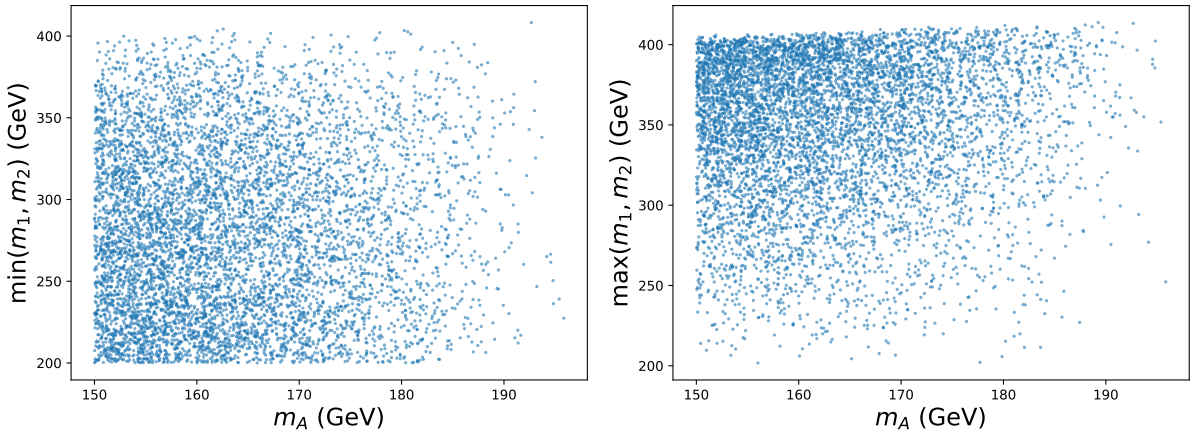

Figure 15: $m_A \simeq m_H$ plotted versus $\min(m_1, m_2)$ (left) and $\max(m_1, m_2)$ (right). The preference for smaller m_A can be seen by the relative over density of points near 150 GeV, and we see that there is no comparable preference for low $m_{1,2}$, as the points are relatively uniform above the constraint $m_{1,2} > 200$ GeV.

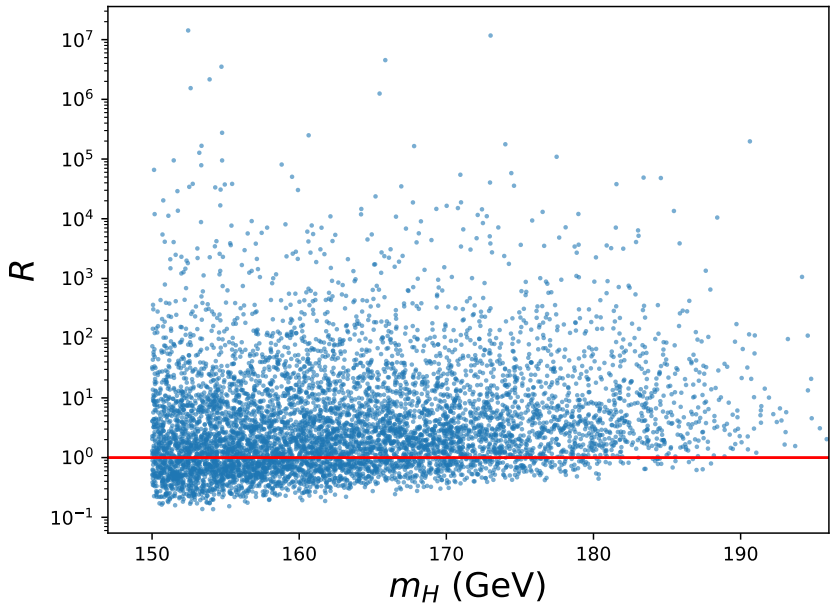

Figure 16: The ratio of partial decay widths, R, as defined in the text, as a function of m_H, showing that most of the parameter space is Z-dominant rather than h_{SM}-dominant, especially for large values of m_H. The red line corresponding to R=1 to guide the eye.

of the cases in the parameter scan $H/A \to Z + V/h_d$ is the dominant decay mode. We also see from the Figure that for $m_H \gtrsim 175$ GeV or so, almost all the parameter space points lead to $R > 1$, so that the decay into $H \to Z + V/h_d$ will dominate. We will refer to the points in parameter space with $R > 1$ as "Z-dominant", and those with $R < 1$ as "h_{SM}-dominant" in the following discussion. Further, in all the cases considered below it will be assumed that both V and h_d will decay invisibly, either to DM or will have a sufficiently long enough lifetimes so as to escape the detector and so lead to MET signatures.

In order to further our understanding of the numerous possibilities within this parameter space, four

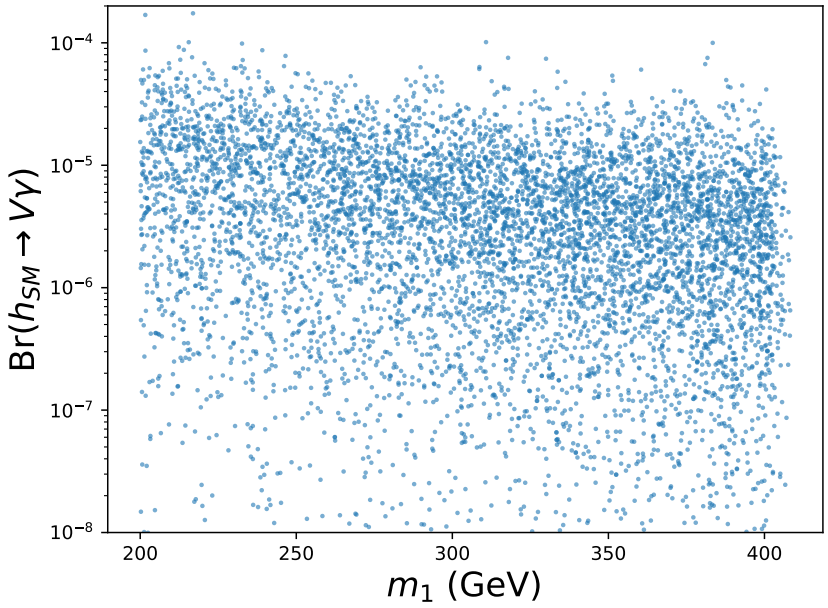

Figure 17: $\mathrm{Br}(h_{SM} \to V\gamma)$, up to an overall factor of $\frac{g_D^2}{e^2}$, vs m_1. Larger m_1 generally decreases the branching fraction of $h_{SM} \to V\gamma$, as expected.

benchmark points(BPs) were selected [6] with either lighter of heavier Higgs states and with either Z-dominant or h_{SM}-dominant decays; these are presented in Table 3. These BPs were then subjected to several recasted LHC searches (for SUSY or DM) which we only briefly discuss here; for a full discussion of analysis details and further information about the benchmark points, see Ref. [6]. As one example to give a flavor of these analyses, an obvious signal channel to consider is that provided by the Z+MET final state which can arise from both the HV and Ah_d associated production. These both occur via Z^* s-channel exchange when both H/A subsequently decay to an on-shell Z which itself then decays to jets or charged leptons. This type of search is clearly most sensitive to model points similar to BP1 and BP2 but other final states, *e.g.*, h_{SM}+MET, are more sensitive to the other pair of benchmarks. It is to be noted that since the final state contains a Z plus two particles each producing MET into opposite hemisphere the *overall* MET is, on average, somewhat reduced making it somewhat easier for points to survive searches with high MET thresholds unless lots of luminosity is available to probe tails of distributions. ATLAS [56, 57] has performed MET searches in the $Z \to$ jet/lepton channels while CMS [58] concentrates on the $Z \to$ leptons channel but also using higher integrated luminosity. Once these searches are recast, the various signal regions are examined to determine which one shows the greatest model sensitivity, *i.e.*, the smallest background in comparison to the anticipated signal rate; in almost all cases examined this results in obtaining a small value for S/B.

Benchmark Point	m_H	m_1	m_2	Z or h_{SM} dominant
BP1	180.8 GeV	371.0 GeV	333.2 GeV	Z
BP2	154.7 GeV	203.9 GeV	249.0 GeV	Z
BP3	187.8 GeV	305.6 GeV	346.2 GeV	h_{SM}
BP4	155.7 GeV	210.5 GeV	275.3 GeV	h_{SM}

Table 3: Four benchmark points and their mass parameter values used to analyze the efficiency of LHC searches for the model. These roughly span the range of m_H, m_1, and m_2 produced by the full parameter scan, with two Z-dominant points and two h_{SM}-dominant points.

Model	$Z(q\bar{q})$+MET [56]	$Z(l^+l^-)$+MET [58]	$h_{SM}(b\bar{b})$+MET [59]	$h_{SM}(\gamma\gamma)$+MET [60]
BP1	13	1.3	–	–
BP2	12	1.0	–	–
BP3	–	–	9	3.8
BP4	–	–	6	2
	W^+W^-+MET [62]	WZ+MET [63]	Wh_{SM}+MET	$h_{SM}(\gamma\gamma)$+MET [69]
BP1	70	8	–	–
BP2	22	6	–	–
BP3	48	–	28 ($b\bar{b}$) [68]	2
BP4	19	–	14 ($\gamma\gamma$) [69]	1.2

Table 4: The ratio $\sigma_{\rm vis,lim}/\sigma_{\rm vis,BPx}$ for the analysis bin providing the strongest constraint arising from the searches for the various final states produced for scalar PM models at the LHC. Note that the limits for $Z \to l^+l^-$+MET are estimates from searches for $Zh_{SM} \to l^+l^-$ + inv. rather than model-independent limits. For final states with multiple searches, here is displayed the result of the search with smallest value of $\sigma_{\rm vis,lim}/\sigma_{\rm vis,BPx}$. The $h_{SM} \to \gamma\gamma$+MET search in the lower half of the table reflects the Category 12 signal region of Ref. [69] applied to $H/A + V/h_d$ associated production events.

The results of this and several other ATLAS and CMS searches applied to the 4 benchmark points is summarized in Table 4. Overall, as noted, the constraints are seen to lie far from the benchmark point predictions with the obvious exception being in the case of the full-luminosity CMS Z+MET search with the Z decaying leptonically. In this case, both BP1 and BP2 yield S/B values which are close to unity implying this is the most sensitive search of the Z-dominant models, which, since they dominate the population overall, implies an ability to probe much of the full parameter space. Clearly, a further far more detailed study of this particular search sensitivity is warranted especially as significant integrated luminosity at 14 TeV is obtained.

In addition to these SUSY-like searches, rare decays of the SM-like Higgs boson, *e.g.*, $h_{SM} \to V\gamma$ (*i.e.*, γ + MET) and $h_{SM} \to Zh_dV$ (*i.e.*, Z+MET), can be used to probe this model parameter space. In the first case, a SM background appears at the level of $B \simeq 3 \cdot 10^{-4}$ due to the process $h_{SM} \to Z\gamma \to \gamma\bar{\nu}\nu$ while for the second process one expects $B \simeq 4.3 \cdot 10^{-3}$ in the SM from $h_{SM} \to ZZ^* \to Z\bar{\nu}\nu$. In the familiar KM approach, the $h_{SM} \to V\gamma$ process proceeds through loops of SM particles via the same graphs as does $h_{SM} \to 2\gamma$ but now a finite KM allows us to make the replacement $\gamma \to V$, hence, this amplitude is always both ϵ as well as loop suppressed. Here, the $h_{SM} \to V\gamma$ process proceeds via the charged Higgs triangle and loop graphs so that only $m_{1,2}$ and g_D/e are unknown factors in the calculation. For this model set the resulting values of the branching fraction are shown in Fig. 17 where we see the predictions all lie quite safely below the expected SM background value when $g_D/e \simeq 1$; this is partly due to the cancellation between the two charged Higgs contributions. The measured upper limit on this branching fraction from the LHC for this process is presently 1.8% from Ref. [71]. In the usual discussion, the process $h_{SM} \to ZV$, which produces a similar final state as does ZVh_d as far as the detector is concerned, can occur at tree level via KM plus mass mixing and so is doubly suppressed by $\sim \epsilon m_V^2/m_Z^2$. Alternatively, this process can proceed via the same SM loops as does $h_{SM} \to Z\gamma$ but with $\gamma \to V$ due to a finite ϵ as above so that it is again doubly suppressed. Here, the $h_{SM} \to Zh_dV$ process occurs at *tree-level* via virtual Z^*, A^* or H^* exchanges, which can interfere destructively, and where the values of t, $m_H = m_A$, g_D/e as well as the trilinear $Hh_{SM}h_d$ coupling, denoted here by $\tilde{\lambda}$, are now the unknowns. The model predictions for the branching fraction can be reasonably sizable in this case, commonly $B \sim 0.1 - 1\%$, particularly if H is light as is shown in Fig. 18, and yield values somewhat comparable to the SM background prediction. For larger values of the rate, it may be possible to partially separate the SM background from the predicted model signal by employing cuts on the reconstructed Z boson energy distribution in the h_{SM} rest frame [6].

It is clear from this brief overview of this rather simple scalar PM scenario with a relatively light mass spectrum that much of the parameter space should be accessible quite soon to LHC analyses and so warrants further study. It would also be interesting to examine a more complex scenario where the

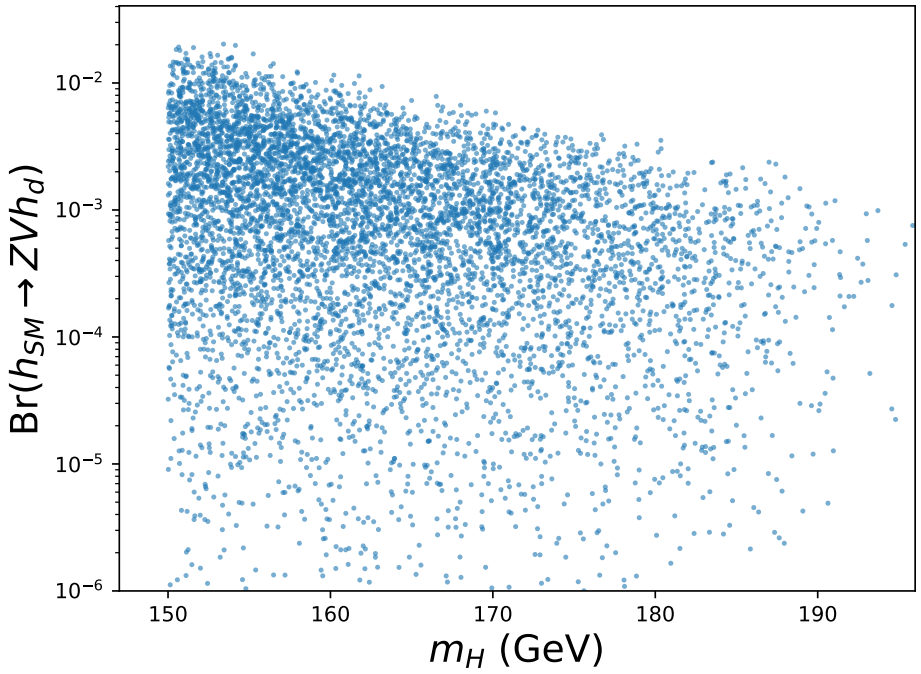

Figure 18: Branching fraction for $h_{SM} \to ZVh_d$ vs. m_H, assuming the SM value of the Higgs width $\Gamma(h_{SM}) = 4.07$ MeV. While the majority of models have $\mathrm{Br}(h_{SM} \to ZVh_d) \simeq 0.01 - 1\%$, it is possible for the branching fraction to be quite suppressed due to small values of $\tilde{\lambda}$ and/or large destructive interference between the three decay amplitudes.

roles of the dark Higgs multiplets and PM are played by different scalar representations.

6 Discussion and Conclusions

Simple renormalizable kinetic mixing models posit that the $U(1)_Y$ hypercharge gauge boson of the SM mixes with the $U(1)_D$ dark photon gauge boson through vacuum polarization-like graphs thus allowing for dark matter to interact with ordinary matter with suppressed couplings. Portal matter particles, which carry both SM and dark sector quantum numbers, play a very pivotal enabling role in these kinetic mixing/dark photon scenarios being necessary to make them function as they are responsible for generating the necessary one-loop graphs. If such particles exist, because they necessarily couple to the SM gauge interactions, the only way that they could have avoided detection so far is if they are relatively massive, $\gtrsim 1$ TeV, and/or decay in an elusive manner. Such particles are likely beyond the direct pair production mass reach of the $\sqrt{s} = 240 - 380$ GeV ILC, FCC-ee or CEPC e^+e^- colliders but can be probed in such machines through indirect tree-level processes. These considerations thus imply that higher energy colliders such as the HL-LHC are the only places where the direct production of such states can be examined and probed in detail. There are some good reasons to expect that at least some of the PM fields, as well as the heavy gauge bosons of an extension of the dark gauge group, may exist in the region of the TeV mass scale, especially when the value of dark gauge coupling, α_D, is large and/or the PM are scalars as their masses are then directly linked to the SM vev, at least in the simplest models. In this White Paper, we have provided an overview of some of the basic PM model components and signatures as well as those for a possible next step up the ladder towards a UV-completion based on an extended dark gauge group which leads to a highly enriched phenomenology and thus to many possible additional collider signatures. This particular path upwards in energy scale is hardly unique and many other scenarios are possible. Not all of these many production processes have been sufficiently well studied and many require much more detailed and realistic simulations especially as the accessible model parameter space continues to grow at the 14 TeV LHC.

PM is a fundamental ingredient of the KM scenario and full implications of its possible existence are in need of further exploration.

Acknowledgements

The author would like to particularly thank J.L. Hewett, D. Rueter and G. Wojcik for very valuable discussions and/or earlier collaboration related to this work. This work was supported by the Department of Energy, Contract DE-AC02-76SF00515.

References

[1] There has been a huge amount of work on this subject; see, for example, D. Feldman, B. Kors and P. Nath, Phys. Rev. D **75**, 023503 (2007) [hep-ph/0610133]; D. Feldman, Z. Liu and P. Nath, Phys. Rev. D **75**, 115001 (2007) [hep-ph/0702123 [HEP-PH]].; M. Pospelov, A. Ritz and M. B. Voloshin, Phys. Lett. B **662**, 53 (2008) [arXiv:0711.4866 [hep-ph]]; M. Pospelov, Phys. Rev. D **80**, 095002 (2009) [arXiv:0811.1030 [hep-ph]]; H. Davoudiasl, H. S. Lee and W. J. Marciano, Phys. Rev. Lett. **109**, 031802 (2012) [arXiv:1205.2709 [hep-ph]] and Phys. Rev. D **85**, 115019 (2012) doi:10.1103/PhysRevD.85.115019 [arXiv:1203.2947 [hep-ph]]; R. Essig *et al.*, arXiv:1311.0029 [hep-ph]; E. Izaguirre, G. Krnjaic, P. Schuster and N. Toro, Phys. Rev. Lett. **115**, no. 25, 251301 (2015) [arXiv:1505.00011 [hep-ph]]; For a general overview and introduction to this framework, see D. Curtin, R. Essig, S. Gori and J. Shelton, JHEP **1502**, 157 (2015) [arXiv:1412.0018 [hep-ph]].

[2] B. Holdom, Phys. Lett. **166B**, 196 (1986) and Phys. Lett. B **178**, 65 (1986); K. R. Dienes, C. F. Kolda and J. March-Russell, Nucl. Phys. B **492**, 104 (1997) [hep-ph/9610479]; F. Del Aguila, Acta Phys.

Polon. B **25**, 1317 (1994) [hep-ph/9404323]; K. S. Babu, C. F. Kolda and J. March-Russell, Phys. Rev. D **54**, 4635 (1996) [hep-ph/9603212]; T. G. Rizzo, Phys. Rev. D **59**, 015020 (1998) [hep-ph/9806397].

[3] T. G. Rizzo, Phys. Rev. D **99**, no.11, 115024 (2019) [arXiv:1810.07531 [hep-ph]].

[4] T. D. Rueter and T. G. Rizzo, Phys. Rev. D **101**, no.1, 015014 (2020) [arXiv:1909.09160 [hep-ph]].

[5] J. H. Kim, S. D. Lane, H. S. Lee, I. M. Lewis and M. Sullivan, Phys. Rev. D **101**, no.3, 035041 (2020) [arXiv:1904.05893 [hep-ph]].

[6] T. D. Rueter and T. G. Rizzo, [arXiv:2011.03529 [hep-ph]].

[7] G. N. Wojcik and T. G. Rizzo, [arXiv:2012.05406 [hep-ph]].

[8] T. G. Rizzo, JHEP **11**, 035 (2021) [arXiv:2106.11150 [hep-ph]].

[9] N. Aghanim *et al.* [Planck Collaboration], arXiv:1807.06209 [astro-ph.CO].

[10] T. R. Slatyer, Phys. Rev. D **93**, no.2, 023527 (2016) [arXiv:1506.03811 [hep-ph]].

[11] H. Liu, T. R. Slatyer and J. Zavala, Phys. Rev. D **94**, no. 6, 063507 (2016) [arXiv:1604.02457 [astro-ph.CO]].

[12] R. K. Leane, T. R. Slatyer, J. F. Beacom and K. C. Ng, Phys. Rev. D **98**, no.2, 023016 (2018) [arXiv:1805.10305 [hep-ph]].

[13] T. G. Rizzo, SLAC-PUB-17628 (work in progress).

[14] J. Alexander *et al.*, arXiv:1608.08632 [hep-ph].

[15] M. Battaglieri *et al.*, arXiv:1707.04591 [hep-ph].

[16] G. Bertone and T. Tait, M.P., Nature **562**, no.7725, 51-56 (2018) [arXiv:1810.01668 [astro-ph.CO]].

[17] P. Schuster, N. Toro and K. Zhou, [arXiv:2112.02104 [hep-ph]].

[18] See, for example, M. Gockeler, R. Horsley, V. Linke, P. E. L. Rakow, G. Schierholz and H. Stuben, Phys. Rev. Lett. **80**, 4119-4122 (1998) [arXiv:hep-th/9712244 [hep-th]].

[19] C. Murgui and K. M. Zurek, [arXiv:2112.08374 [hep-ph]].

[20] J. de Blas, M. Ciuchini, E. Franco, A. Goncalves, S. Mishima, M. Pierini, L. Reina and L. Silvestrini, [arXiv:2112.07274 [hep-ph]].

[21] M. S. Chanowitz, M. A. Furman and I. Hinchliffe, Phys. Lett. B **78**, 285 (1978)

[22] See, for example, C. Y. Chen, S. Dawson and E. Furlan, Phys. Rev. D **96**, no.1, 015006 (2017) doi:10.1103/PhysRevD.96.015006 [arXiv:1703.06134 [hep-ph]].

[23] M. S. Chanowitz and M. K. Gaillard, Nucl. Phys. B **261**, 379 (1985); B. W. Lee, C. Quigg and H. B. Thacker, Phys. Rev. D **16**, 1519 (1977); J. M. Cornwall, D. N. Levin and G. Tiktopoulos, Phys. Rev. D **10**, 1145 (1974) Erratum: [Phys. Rev. D **11**, 972 (1975)]; G. J. Gounaris, R. Kogerler and H. Neufeld, Phys. Rev. D **34**, 3257 (1986).

[24] B. Batell, M. Pospelov and A. Ritz, Phys. Rev. D **79**, 115008 (2009) [arXiv:0903.0363 [hep-ph]].

[25] N. Arkani-Hamed and N. Weiner, JHEP **0812**, 104 (2008) [arXiv:0810.0714 [hep-ph]]; M. Baumgart, C. Cheung, J. T. Ruderman, L. T. Wang and I. Yavin, JHEP **0904**, 014 (2009) [arXiv:0901.0283 [hep-ph]]; A. Falkowski, J. T. Ruderman, T. Volansky and J. Zupan, Phys. Rev. Lett. **105**, 241801 (2010) [arXiv:1007.3496 [hep-ph]] and JHEP **1005**, 077 (2010) [arXiv:1002.2952 [hep-ph]]; C. Cheung, J. T. Ruderman, L. T. Wang and I. Yavin, JHEP **1004**, 116 (2010) [arXiv:0909.0290 [hep-ph]]; G. Barello, S. Chang, C. A. Newby and B. Ostdiek, Phys. Rev. D **95**, no. 5, 055007 (2017) [arXiv:1612.00026 [hep-ph]].

[26] G. Guedes and J. Santiago, JHEP **01**, 111 (2022) [arXiv:2107.03429 [hep-ph]].

[27] A. Osman Acar, O. E. Delialioglu and S. Sultansoy, [arXiv:2103.08222 [hep-ph]].

[28] F. Baspehlivan, B. Dagli, O. E. Delialioglu and S. Sultansoy, [arXiv:2201.08251 [hep-ph]].

[29] N. Kumar and S. P. Martin, Phys. Rev. D **92**, no.11, 115018 (2015) [arXiv:1510.03456 [hep-ph]].

[30] P. N. Bhattiprolu and S. P. Martin, Phys. Rev. D **100**, no.1, 015033 (2019) doi:10.1103/PhysRevD.100.015033 [arXiv:1905.00498 [hep-ph]].

[31] J. L. Hewett and T. G. Rizzo, Phys. Rept. **183**, 193 (1989)

[32] H. Baer, T. Barklow, K. Fujii, Y. Gao, A. Hoang, S. Kanemura, J. List, H. E. Logan, A. Nomerotski and M. Perelstein, *et al.* [arXiv:1306.6352 [hep-ph]].

[33] A. Abada *et al.* [FCC], Eur. Phys. J. ST **228**, no.2, 261-623 (2019).

[34] J. B. Guimarães da Costa *et al.* [CEPC Study Group], [arXiv:1811.10545 [hep-ex]].

[35] For some recent work and original references, see V. I. Telnov, JINST **15**, no.10, P10028 (2020) [arXiv:2007.14003 [physics.acc-ph]].

[36] J. P. Lees *et al.* [BaBar], Phys. Rev. Lett. **119**, no.13, 131804 (2017) [arXiv:1702.03327 [hep-ex]].

[37] M. Campajola [Belle-II], Phys. Scripta **96**, no.8, 084005 (2021)

[38] This is well-known in the case of, *e.g.*, SUSY searches; see, for example, H. K. Dreiner, O. Kittel and U. Langenfeld, Eur. Phys. J. C **54**, 277-284 (2008) [arXiv:hep-ph/0703009 [hep-ph]].

[39] E. W. N. Glover and J. J. van der Bij, Nucl. Phys. B **321**, 561-590 (1989)

[40] G. Jikia, Nucl. Phys. B **405**, 24-54 (1993)

[41] F. Přeučil and J. Hořejší, J. Phys. G **45**, no.8, 085005 (2018) [arXiv:1707.08106 [hep-ph]].

[42] J. Quevillon, C. Smith and S. Touati, Phys. Rev. D **99**, no.1, 013003 (2019) [arXiv:1810.06994 [hep-ph]].

[43] P. De Fabritiis, P. C. Malta and J. A. Helayël-Neto, Phys. Rev. D **105**, no.1, 016007 (2022) [arXiv:2109.12245 [hep-ph]].

[44] M. Ghasemkhani, V. Rahmanpour, R. Bufalo and A. Soto, [arXiv:2109.11411 [hep-th]].

[45] T. G. Rizzo, in preparation.

[46] We employ numerical estimates based on M. Czakon and A. Mitov, Comput. Phys. Commun. **185**, 2930 (2014) [arXiv:1112.5675 [hep-ph]] and also M. Aliev, H. Lacker, U. Langenfeld, S. Moch, P. Uwer and M. Wiedermann, Comput. Phys. Commun. **182**, 1034 (2011) doi:10.1016/j.cpc.2010.12.040 [arXiv:1007.1327 [hep-ph]]. bibitemhpair We employ numerical estimates based on M. Czakon and A. Mitov, Comput. Phys. Commun. **185**, 2930 (2014) [arXiv:1112.5675 [hep-ph]] and also M. Aliev, H. Lacker, U. Langenfeld, S. Moch, P. Uwer and M. Wiedermann, Comput. Phys. Commun. **182**, 1034 (2011) doi:10.1016/j.cpc.2010.12.040 [arXiv:1007.1327 [hep-ph]].

[47] A. Leike, Phys. Rept. **317**, 143-250 (1999) [arXiv:hep-ph/9805494 [hep-ph]].

[48] T. G. Rizzo, [arXiv:hep-ph/0610104 [hep-ph]].

[49] P. Langacker, Rev. Mod. Phys. **81**, 1199-1228 (2009) doi:10.1103/RevModPhys.81.1199 [arXiv:0801.1345 [hep-ph]].

[50] G. Aad *et al.* [ATLAS Collaboration], arXiv:1903.06248 [hep-ex].

[51] ATLAS Collaboration, "Prospects for searches for heavy Z' and W' bosons in fermionic final states with the ATLAS experiment at the HL-LHC", ATL-PHYS-PUB-2018-044.

[52] M. Aaboud *et al.* [ATLAS], JHEP **01**, 055 (2018) [arXiv:1709.07242 [hep-ex]].

[53] ATLAS Collaboration, "Prospects for the search for additional Higgs bosons in the ditau final state with the ATLAS detector at HL-LHC", ATL-PHYS-PUB-2018-050

[54] For a classic review and original references, see R.N. Mohapatra, Unification and Supersymmetry, (Springer, New York,1986).

[55] M. Aaboud *et al.* [ATLAS], JHEP **01**, 126 (2018) [arXiv:1711.03301 [hep-ex]].

[56] M. Aaboud *et al.* [ATLAS Collaboration], JHEP **2018**, 180 (2018) [arXiv:1807.11471 [hep-ex]].

[57] ATLAS Collaboration, Phys. Lett. B **776**, 318 (2018) [arXiv:1708.09624 [hep-ex]].

[58] A. M. Sirunyan *et al.* (CMS Collaboration), Eur. Phys. J. C 81 (2021) 13; Erratum: Eur. Phys. J. C 81 (2021) 333 [arXiv:2008.04735 [hep-ex]].

[59] M. Aaboud *et al.* (ATLAS Collaboration), Phys. Rev. Lett. **119**, 181804 (2017) [arXiv:1707.01302 [hep-ex]].

[60] M. Aaboud *et al.* (ATLAS Collaboration), Phys. Rev. D **96**, 112004 (2017) [arXiv:1706.03948 [hep-ex]].

[61] ATLAS Collaboration, ATL-PHYS-PUB-2016-012.

[62] G. Aad *et al.* (ATLAS Collaboration), Eur. Phys. J. C **80**, 123 (2020) [arXiv:1908.08215 [hep-ex]].

[63] M. Aaboud *et al.* (ATLAS Collaboration), Eur. Phys. J. C **78**, 995 (2018) [arXiv:1803.02762 [hep-ex]].

[64] G. Aad *et al.* (ATLAS Collaboration), JHEP **2014**, 169 (2014) [arXiv:1402.7029 [hep-ex]].

[65] G. Aad *et al.* (ATLAS Collaboration), JHEP **2014**, 71 (2014) [arXiv:1403.5294 [hep-ex]].

[66] G. Aad *et al.* (ATLAS Collaboration), Phys. Rev. D **101**, 052005 (2020) [arXiv:1911.12606 [hep-ex]].

[67] G. Aad *et al.* (ATLAS Collaboration), Phys. Rev. D **101**, 072001 (2020) [arXiv:1912.08479 [hep-ex]].

[68] G. Aad *et al.* (ATLAS Collaboration), Eur. Phys. J. C **80**, 691 (2020) [arXiv:1909.09226 [hep-ex]].

[69] G. Aad *et al.* (ATLAS Collaboration), JHEP **2020**, 5 (2020) [arXiv:2004.10894 [hep-ex]].

[70] G. Aad *et al.* [ATLAS], Phys. Lett. B **809**, 135754 (2020) [arXiv:2005.05382 [hep-ex]].

[71] G. Aad *et al.* [ATLAS], [arXiv:2109.00925 [hep-ex]].